Report 11, 1990

APPLICATION OF SCHLUMBERGER SOUNDING AT EBURRU, KENYA AND TEM AND MT METHODS AT BAKKI, S-ICELAND

Stephen Alumasa Onacha,
UNU Geothermal Training Programme,
Orkustofnun - National Energy Authority,
Grensásvegur 9,
108 Reykjavik,
ICELAND

Permanent address:
Olkaria Geothermal,
P. O. Box 785,
Naivasha,
KENYA

ABSTRACT

The 2-D Schlumberger and the combined 1-D TEM/MT sounding interpretations have given results that relate to permeability, temperature, degree of hydrothermal alteration, and geological and structural features of Eburru and Bakki geothermal fields.

The 2-D interpretation of Schlumberger sounding data from Eburru, Kenya has identified two anomalous areas of low resistivity ($\leq$ 10 Ωm) at 1000 m a.s.l. The first anomaly is in the Eburru crater area which is currently under exploratory drilling. The low resistivity seems to define an area of interpolated reservoir temperature of 200°C. The low resistivity above 1800 m a.s.l. is caused by hydrothermal alteration of pyroclastics by acidic steam condensates and lateral outflows mainly to the northwest, northeast and south along faultlines. The low resistivity area has sharp boundaries. Outside this area the resistivity is higher ($\geq$ 30 Ωm) due to low permeability and temperature which has been confirmed by exploration wells. The second anomaly is found in the Badlands in association with a gravity high and a magnetic low. The two areas are separated by high resistivity and an E-W structural discontinuity. The depth to the bottom of the low resistivity is not defined.

The combined interpretation of 1-D TEM and MT sounding data at Bakki and a comparison with well data shows that the surface low resistivity layer corresponds to a permeable layer of hyaloclastites, temperatures of 100° to 150°C and laumontite - wairakite alteration mineralogy. The low resistivity layer is thicker at Bakki which is probably related to upflow of geothermal fluids. A thick ($\geq$ 4 km) high resistivity layer ($\geq$ 100 Ωm) is found below the low resistivity layer. A conductive layer ($\leq$ 5 Ωm) at a depth of more than 5 km has been identified at Bakki. This layer may be related to the heat source of the geothermal system.

The TEM/MT data interpretation has also given an indication of the problem of static shifts in MT data due to near-surface inhomogeneities. The MT data is shifted by more than one order of magnitude.

LIST OF CONTENTS

LIST OF FIGURES

1. INTRODUCTION

1.1 Scope of work

This report presents the work of the author in the last two and a half months of the UNU Geothermal Training Programme in Iceland. The report presents the two dimensional interpretation of 2-D Schlumberger soundings from Eburru, Kenya and the application and interpretation of the central loop transient electromagnetic method (CLTEM) and audiomagnetotelluric and magnetotelluric (AMT/MT) soundings from Bakki, S-Iceland. A brief overview of theoretical aspects of the methods in their application in geothermal exploration is given. An attempt is made to relate the modelled geophysical parameters to the geological and tectonic structures and the physio-chemical characteristics of these geothermal fields.

1.2 Application of resistivity methods in geothermal exploration

Electrical resistivity methods have proven to be very useful in geothermal exploration because they relate directly to the properties of interest such as temperature, effective porosity and the degree of hydrothermal alteration of the rocks.

The most common methods are DC resistivity sounding, especially with the Schlumberger electrode configuration and the magnetotelluric (MT) methods. In the DC method, an electrical current is injected into the earth and the potential signal generated by the current distribution is measured on the surface. In the MT method, the current in the ground is induced by the time varying electromagnetic field. Orthogonal components of the magnetic and electric fields are measured. Transient electromagnetic methods (TEM) have recently gained popularity and may replace the DC resistivity sounding method in geothermal exploration. In the TEM method, the current is induced by a time varying magnetic field generated by a loop or a grounded dipole and the decaying induced magnetic field is monitored at the surface.

The basic problem in these methods is the non-uniqueness in the modelled parameters. A combined interpretation approach gives a better resolution of the sub-surface parameters. The TEM method gives a better resolution of conductive layers while the DC method is more sensitive to resistive structures. The MT method is better suited for investigation of deeper regional structures. The TEM method may be used to correct for static shifts inherent in MT data.

1.3 Resistivity of rocks

The electrical resistivity of rocks varies tremendously depending on the origin and the physio-chemical properties of the rocks. The bulk resistivity ρ is related to porosity (especially fracture porosity and pore structure), temperature and pressure, geological structure, the degree of hydrothermal alteration of the rocks, fluid saturation and salinity. For saturated rocks where ionic conduction is dominant, the bulk resistivity is related to porosity ϕ_t and the resistivity ρ_w of the pore fluid through Archie's law.

$$F = \rho / \rho_w = a \, \phi_t^{-n} \tag{1.1}$$

Where F is the formation factor, a and n are constants which may be determined empirically. The increase in resistivity with an increase in temperature and/or pressure for saturated samples (Drury and Hyndman, 1979) gives evidence of pore fluid conduction. In dehydrated rocks,

conduction is mainly through mineral grains. The pore fluid resistivity for temperatures between 150°-200°C may be approached as

$$\rho_w = \rho_{w0} / (1 + \alpha(T-T_0)), \tag{1.2}$$

where ρ_{w0} is the resistivity of the fluid at temperature T_o, and α is the temperature coefficient of resistivity at T_0.

In basalts, the bulk resistivity is also affected by interface conduction, mainly due to the presence of clay minerals along fractures. The interface conduction is more important where pore fluid resistivity exceeds approximately 5 Ωm, while pore fluid conduction dominates for pore fluid resistivity values of 1 Ωm or lower (Flovenz et al., 1985).

2. 2-D MODELLING OF SCHLUMBERGER SOUNDINGS FROM EBURRU, KENYA

2.1 Introduction

The Eburru geothermal field is situated within the Eburru volcanic complex of the Kenya Rift Valley (Figure 1). The volcanic complex has two major volcanic centres arranged in an E-W direction. The present exploration area is a part of the eastern volcanic centre that has many craters and faults. There are two major fault systems: the NNW-SSE trending old rift faults and the younger N-S faults which form a graben structure with young rhyolitic lava flows, craters, fumaroles and steaming grounds. The Eburru area is mostly covered by pyroclastics with some outcrops of rhyolite, obsidian, trachytes, basalts and tuffs of Miocene-Pliocene age (Figure 2).

Geothermal exploration has been carried out in Eburru since 1972 when the UNDP completed a survey of the area along with several other prospects in Kenya. In 1983, JICA also made a study of the geothermal activity of the northern part of Eburru. Previous geophysical work carried out in this area include the roving dipole (Group Seven Inc., 1972), gravity (Simiyu, 1990), aeromagnetic survey (Figure 3) and S-P measurements (KPC, 1986). A total of 125 DC Schlumberger soundings with a maximum current electrode spacing of 6000 m and 363 profiling stations have been made, covering an area of 850 square kilometres.
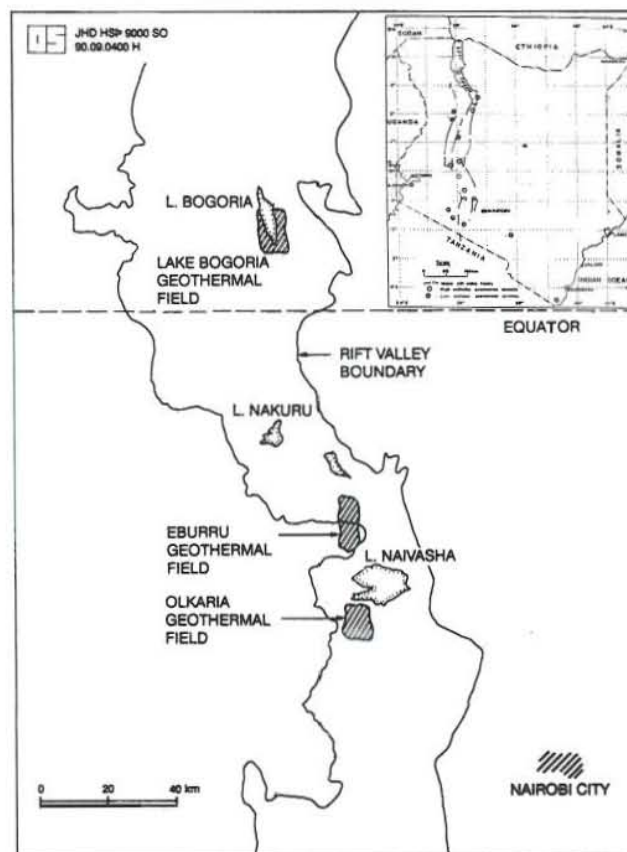
FIGURE 1: The location of the Eburru geothermal field in the Kenya Rift Valley
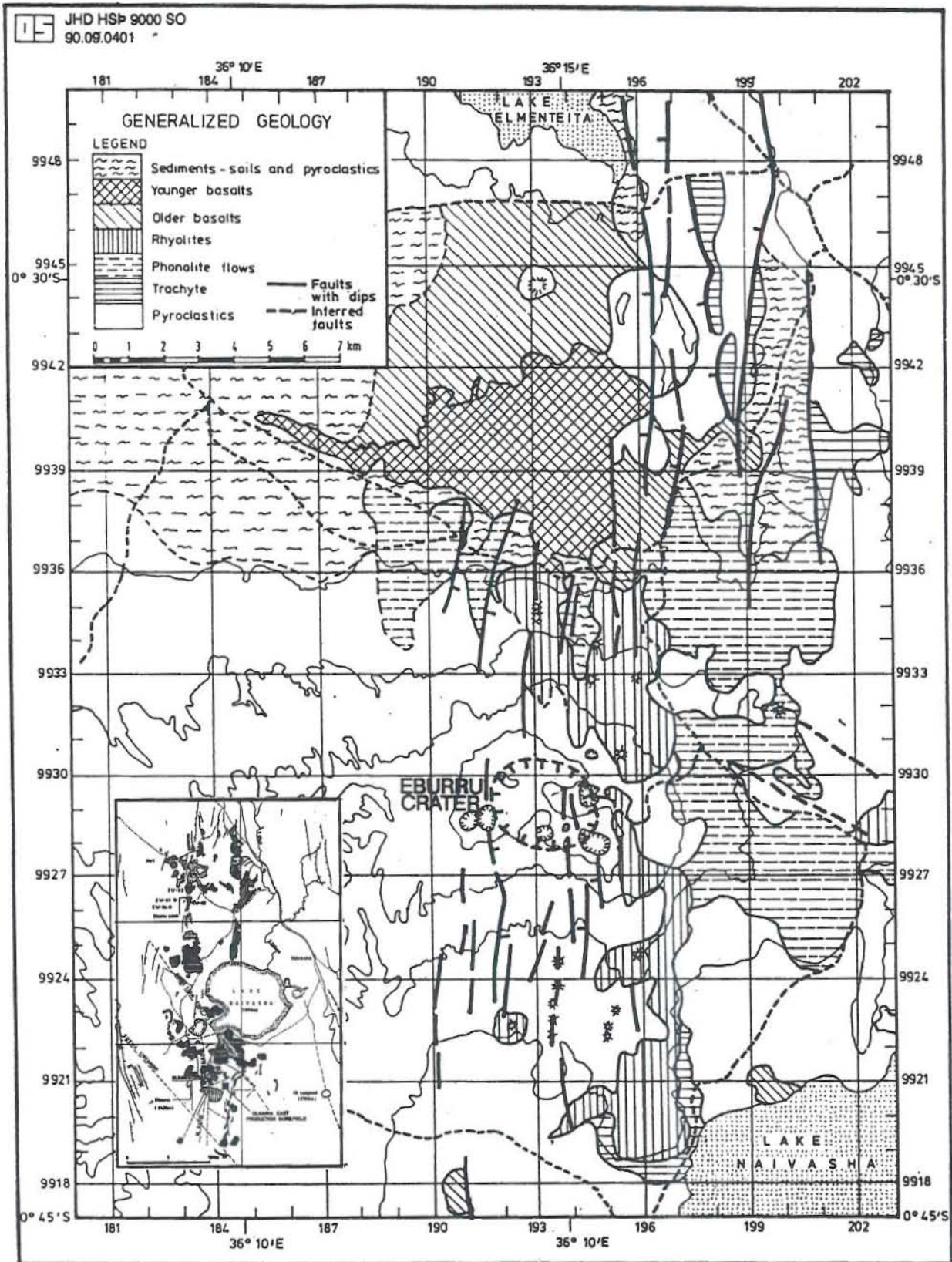
FIGURE 2: Simplified geological map of the Eburru-Badlands area

Based on a qualitative interpretation of aeromagnetic data by KPC (1986), it was proposed that the broad magnetic high over the Eburru area is caused by deep hydrothermal alterations while the strong negative anomaly to the north of Eburru in the Badlands is caused by near-surface basalts, together with a deeper body. The E-W or NW-SE orientation of the magnetic anomalies tends to suggest a relationship to old faulting trends. However, the dipolar nature of the anomalies in the Rift Valley (Figure 3) has been a major obstacle in the interpretation of the data.
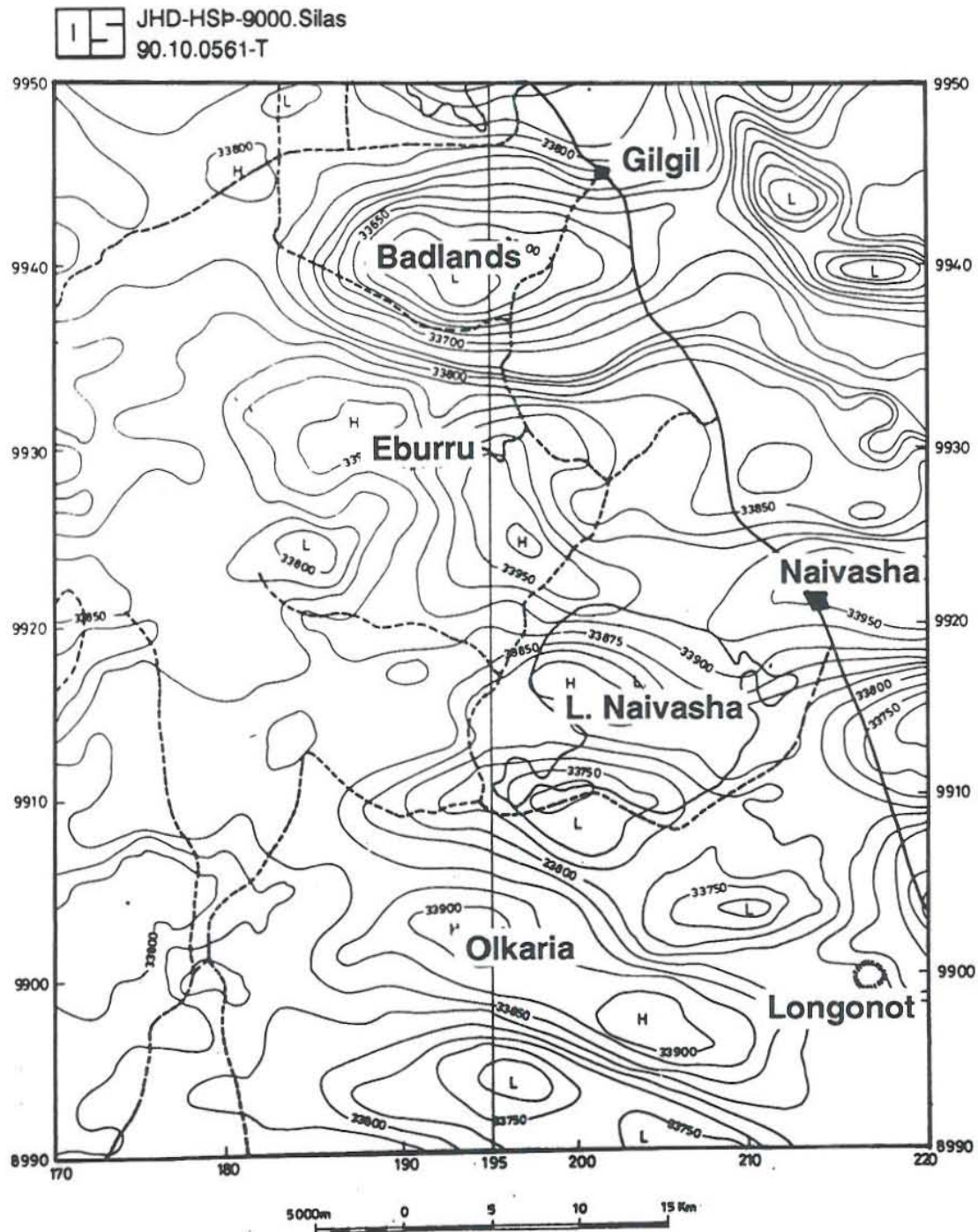
FIGURE 3: The total magnetic anomaly map of the Olkaria-Eburru-Badlands area

Recent gravity measurements (Simiyu, 1990) indicate that the area has a general NE-SW trending gravity low, probably due to a cover of pyroclastics and tuffs. The Eburru field is located on a gravity high with a localized occurrence of gravity lows. The field is separated from the Badlands area in the north by a NW-SE trending structural discontinuity.

Four exploratory wells have been drilled in this area. Three of the wells, EW2, EW3 and EW4 are cold wells, while EW1 is productive with a capacity of about 2.5 MWe. The highest temperature recorded in EW1 is 280°C. The wells have encountered some syenitic intrusions at the bottom.

2.2   Theory of DC Schlumberger sounding

In the Schlumberger method, two potential and two current electrodes are arranged symmetrically around a midpoint. A current (I) is injected through the current electrodes while the potential difference (ΔV) is measured between the potential electrodes. For an inhomogeneous earth, the apparent resistivity ρ_a is defined as

$$\rho_a = \Delta V/I \ \ \pi(S^2 - P^2)/2P, \tag{2.1}$$

where S = half the current electrode spacing, and P is half the potential electrode spacing.

The derivation of the expressions of the potential field due to a point current source at the surface of a horizontally layered earth is carried out by considering the relationship between the current density, the electric field intensity and resistivity. If we assume isotropic horizontal layering with the last layer N of infinite thickness, the general solution for potential in any given layer is defined by:

$$V_i(r,z) = \rho_1 I/2\pi \int_0^\infty \{C_i(\lambda) \cosh[\lambda(z - h_i)] + D_i(\lambda) \sinh[\lambda(z - h_i)]\} J_0 \ \lambda r \ d\lambda, \tag{2.2}$$

where C_i and D_i are determined recursively in terms of resistivity and thickness of the layers. J_0 is the Bessel function of order zero and λ is a variable of integration, ρ_1 is the resistivity of the first layer and h_i is the depth to the ith layer. The functions C_i and D_i are determined by imposing the following boundary conditions:

(a)   The potential $V \rightarrow 0$ as $z \rightarrow \infty$ and $r \rightarrow \infty$.

(b)   The potential is continuous at each of the boundary planes between layers,
         i.e. $V_i = V_{i+1}$.

(c)   The vertical component of the current density is continuous at the boundaries of layers,
         i.e.
         $(1/\rho_i) \ (\partial V_i / \partial z) = (1/\rho_{i+1}) \ (\partial V_{i+1} / \partial z)$ at $z = h_i$.

(d)   The current density is $J_z = \sigma \ \partial V / \partial z = 0$ at the surface layer, except near the current
         source.

By considering boundary condition (b), we see that at $z = h_{i+1}$

$$C_{i+1} = C_i \cosh(\lambda d_i) + D_i \sinh(\lambda d_i), \tag{2.3}$$

where $(h_{i+1} - h_i) = d_i$.

Similarly, for boundary condition (c)

$$D_{i+1} = [C_i \sinh(\lambda d_i) + D_i \cosh(\lambda d_i)] \, \rho_{i+1} / \rho_i, \tag{2.4}$$

and for the Nth layer, $V_N \to 0$ as $z \to \infty$ so that from Equation 2.2,

$$D_N = -C_N.$$

By defining $K_i = -C_i / D_i$, we have $K_N = 1$ and

$$K_i = [K_{i+1} + (\rho_i / \rho_{i+1}) \tanh(\lambda d_i)] / [(\rho_i / \rho_{i+1}) + K_{i+1} \tanh(\lambda d_i)]. \tag{2.5}$$

This is a recursive formula. For the uppermost layer, boundary condition (d) can be shown to imply that $D = -1$ and

$$V_1(r,z) = I \, \rho_1 / 2\pi \int_0^\infty [K_1 \cosh(\lambda z) - \sinh(\lambda z)] \, J_0(\lambda r) \, d\lambda, \tag{2.6}$$

and at the surface ($z = 0$), we have

$$V_1(r,z) = I\rho_1 / 2\pi \int_0^\infty K_1 \, J_0(\lambda r) \, d\lambda. \tag{2.7}$$

Equations 2.5 and 2.7 form the basis for 1-dimensional interpretation of DC soundings.

When the potential electrode spacing is increased, there frequently appear shifts in the apparent resistivity curve. These shifts are often a severe problem in the interpretation of Schlumberger soundings. There are basically two types of shifts. The convergent shifts are due to large resistivity contrasts between layers in horizontally stratified earth. These shifts are greatest where S-P is the same order of magnitude as the depth to the boundary between the layers (Arnason, 1984). These shifts also increase with increasing resistivity contrasts. The nonconvergent shifts are caused by lateral resistivity variations at the centre of the array.

2.3 Data analysis

The initial 2-D model was based on the 1-D interpretation of the Schlumberger soundings. The author reinterpreted Schlumberger soundings around Eburru (Figure 4) using the program ELLIPSE which was written at Orkustofnun. This is a non-linear least square inversion program which uses the Levenberg-Marquart iteration algorithm. The program simulates the actual electrode configuration used in the field by computing the potential at each potential electrode. The shifts due to lateral inhomogeneities close to the centre of the sounding are automatically removed, and all segments tied in with the longest potential electrode spacing (400 m). The results of 1-D inversions are presented along a N-S profile through the Eburru field and on iso-resistivity contour maps for 1800 m a.s.l. and 1000 m a.s.l.

The 2-D modelling was carried out for the N-S profile by the program FELIX which uses a finite element algorithm for modelling arbitrarily shaped two-dimensional resistivity structures with surface topography. The program is basically divided into two parts. The first part is used for entering, changing and plotting model parameters, while the second part is for calculation. A 1:50,000 map with a contour interval of 20 m was used to generate the topography. This implies that topographic surface inhomogeneities are poorly resolved. There is good data coverage around the Eburru peak but sparse data at the southern and northern boundaries of the profile.
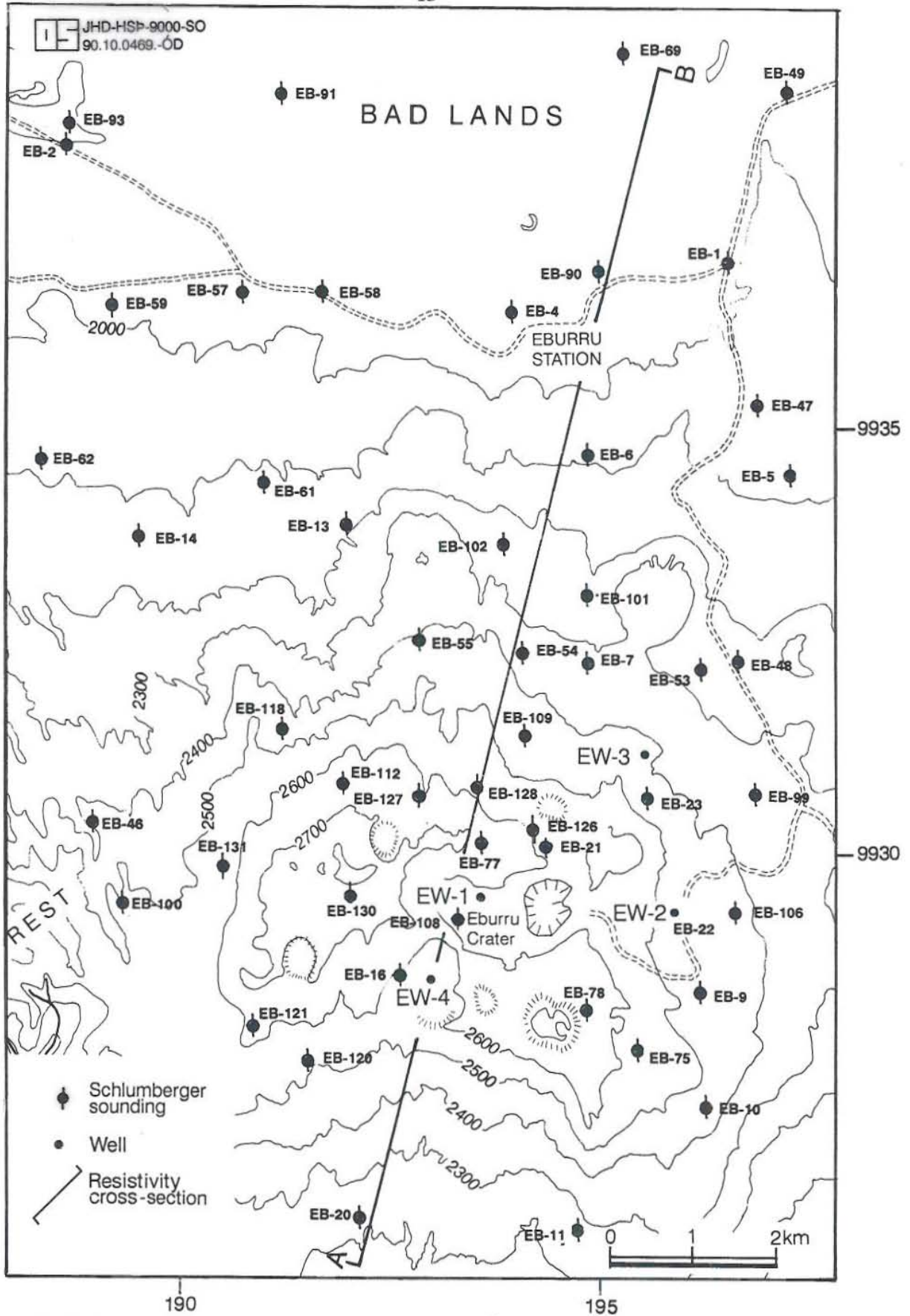
FIGURE 4: Location of DC Schlumberger soundings in the Eburru-Badlands area

The initial vertical and horizontal boundaries were based on the 1-D resistivity structure. The basis of the model is a grid of semi-horizontal and vertical lines. These lines intersect at nodes and form quadrilaterals called elements. The quadrilaterals can be sub-divided into triangles by diagonal lines. Each element is assigned a resistivity index corresponding to a particular resistivity value. A group of connected elements with the same resistivity index defines a resistivity structure or sub-domain. The nodes are numbered to facilitate manipulation of the variations in the shape of sub-domains. The size of elements is altered by changing the positions of nodes, while the resistivity is changed by varying the values of resistivity indices (Figure 5).
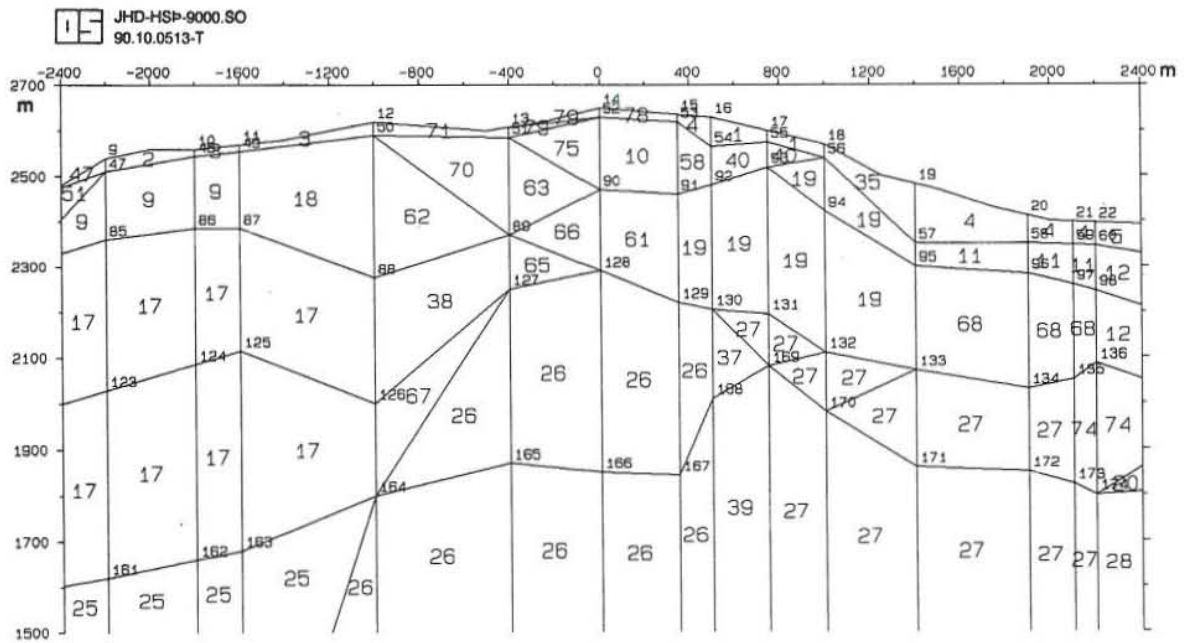
FIGURE 5: An example of the 2-D finite element resistivity grid

A grid generator subdivides the resistivity model into a triangular grid whose dimensions increase quadratically both with depth and laterally outside the traversed area (Figure 6). The program simultaneously computes the responses for Schlumberger soundings, head-on resistivity profiles and co-linear dipoles from a given 2-D resistivity model. The program utilizes a maximum of 10 Schlumberger soundings.

The response of the model is calculated and the results compared to the field data. The initial stages of the modelling were devoted to fitting the surface layer parameters, taking into account the shape and shifts of the field data. After a reasonable fit was obtained, only the 100, 200 and 400 m potential electrode spacings were used for modelling the deeper layers. The calculated curves, based on the final 2-D models with a comparison to the field data, are presented in Appendix A, together with the final model.

JHD-HSÞ-9000.SO
90.10.0514-T
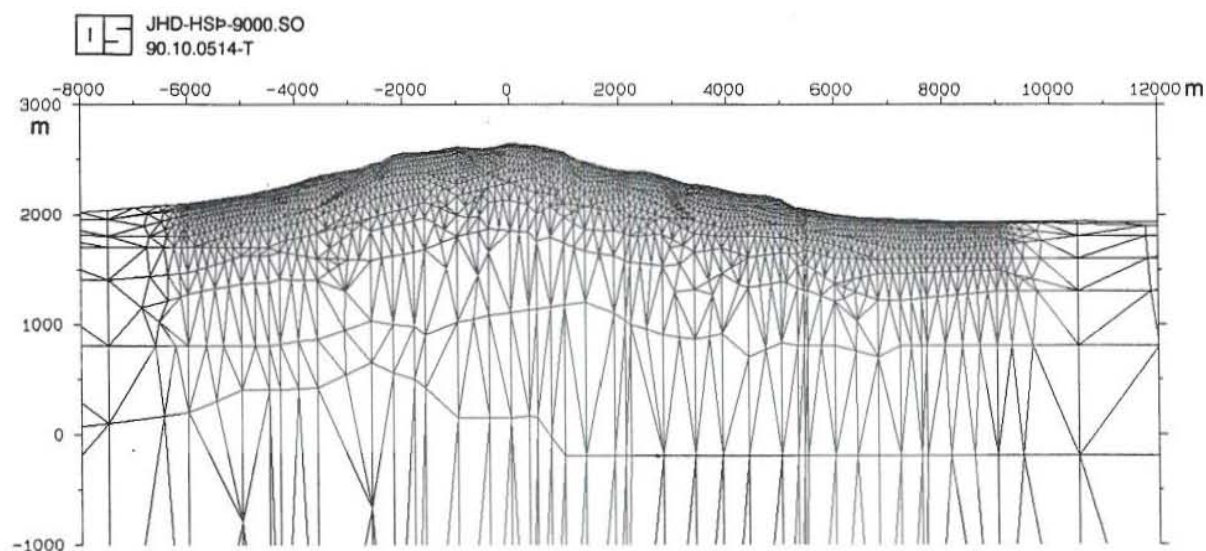
FIGURE 6:   The 2-D finite element grid subdivided into a triangular grid

2.4   Interpretation of results

2.4.1   1-D interpretation

The 1-D interpretation of profile AB (Figure 7) shows that the subsurface in the Ndabibi-Eburru-Badlands area has a wide variation of resistivity values.   The exact locations of vertical and horizontal boundaries are not well defined.   The important features are:

a)   The resistivity of the surface layer varies between 100 - 10,000 Ωm with the highest resistivity values in the Badlands.   The thickness varies from 20 - 250 m.

JHD HSÞ 900 SO
90.10.0447 ÓD
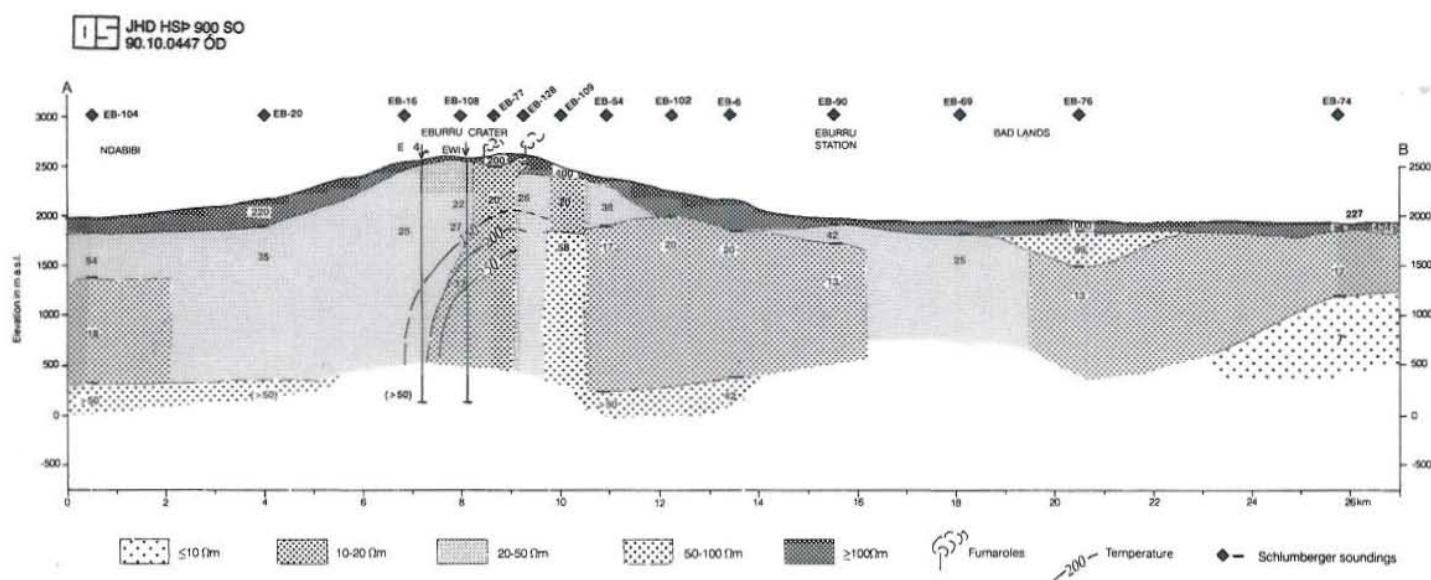
FIGURE 7:   1-D resistivity section along profile AB in the Eburru-Badlands area

b)   There are four different areas of low resistivity (10 - 20 Ωm). These are: the Ndabibi area, the Eburru crater, around the Eburru station, and the Badlands. The Eburru crater area occurs as a narrow conduit whose depth is not well resolved. This anomaly comes close to the surface between soundings EB108 and EB128.

c)   The low resistivity areas are separated by zones of intermediate resistivity (20 - 100 Ωm). Similar resistivity values also occur at depth to the south and north of the Eburru crater. However, the depth and resistivity of this layer are poorly defined.

d)   A extensive layer of low resistivity (≤10 Ωm) is found in the Badlands area below 1000 m a.s.l.

The resistivity map at 1800 m a.s.l. (Figure 8) shows three areas of low resistivity (≤ 20 Ωm). These are found in the Eburru crater area and the Eburru station-Badlands-Oljorai area. The Eburru crater area anomaly has extensions to the northwest, northeast and south around EB11. The values (≤10 Ωm) are found around sounding EB28 and close to well EW3. These outliers may represent near-surface outflows whose surface manifestations are fumaroles along N-S faults. The Badlands anomaly extends in a NW-SE direction with outliers to the south of the Eburru station. The low resistivity areas are separated by an area of intermediate resistivity.

The map at 1000 m a.s.l (Figure 9) indicates the same general features as Figure 8 except that the low resistivity around the Eburru crater is confined by areas of intermediate resistivity. The Badlands-Eburru station anomaly extends in an E-W direction to the Oljorai Ranch where very low resistivity (< 10 Ωm) is found at depth.

2.4.2   2-D interpretation

Figure 10 shows similar features as those of 1-D interpretation. However, the 2-D interpretation gives a better resolution of resistivity values and the location of vertical and some of the horizontal boundaries. This is exemplified by a bigger contrast in the resistivity values. The 2-D interpretation shows the following features:

a)   There are three areas of low resistivity (≤ 10 Ωm). The first area is under the Eburru crater with a shallow extension to the north around EB128. The second is found to the south of Eburru station around EB54. The third area is found in the Badlands. The thickness of this layer is poorly defined, although there are indications of higher resistivity at depth.

b)   The 10 - 20 Ωm layer extends northwards to the Eburru station. This layer is deeper between EB54 and EB102 and also around the Eburru Station, where its depth is not well resolved. This layer is closer to the surface around the crater area.

c)   The areas of low resistivity are separated by areas of intermediate resistivity (20 -100 Ωm) and the boundaries are sharp, especially between EB77 and EB28. There is good resolution of the intermediate resistivity layers at depth, both to the north and south of the Eburru crater area.

The 2-D interpretation gives good evidence of high resistivity around the Eburru geothermal field. The results also indicate a good correlation with 1-D modelling but give high resistivity contrasts, (lower values for low resistivity areas and higher values for resistive areas) and a better resolution of the depths to the layer interfaces.
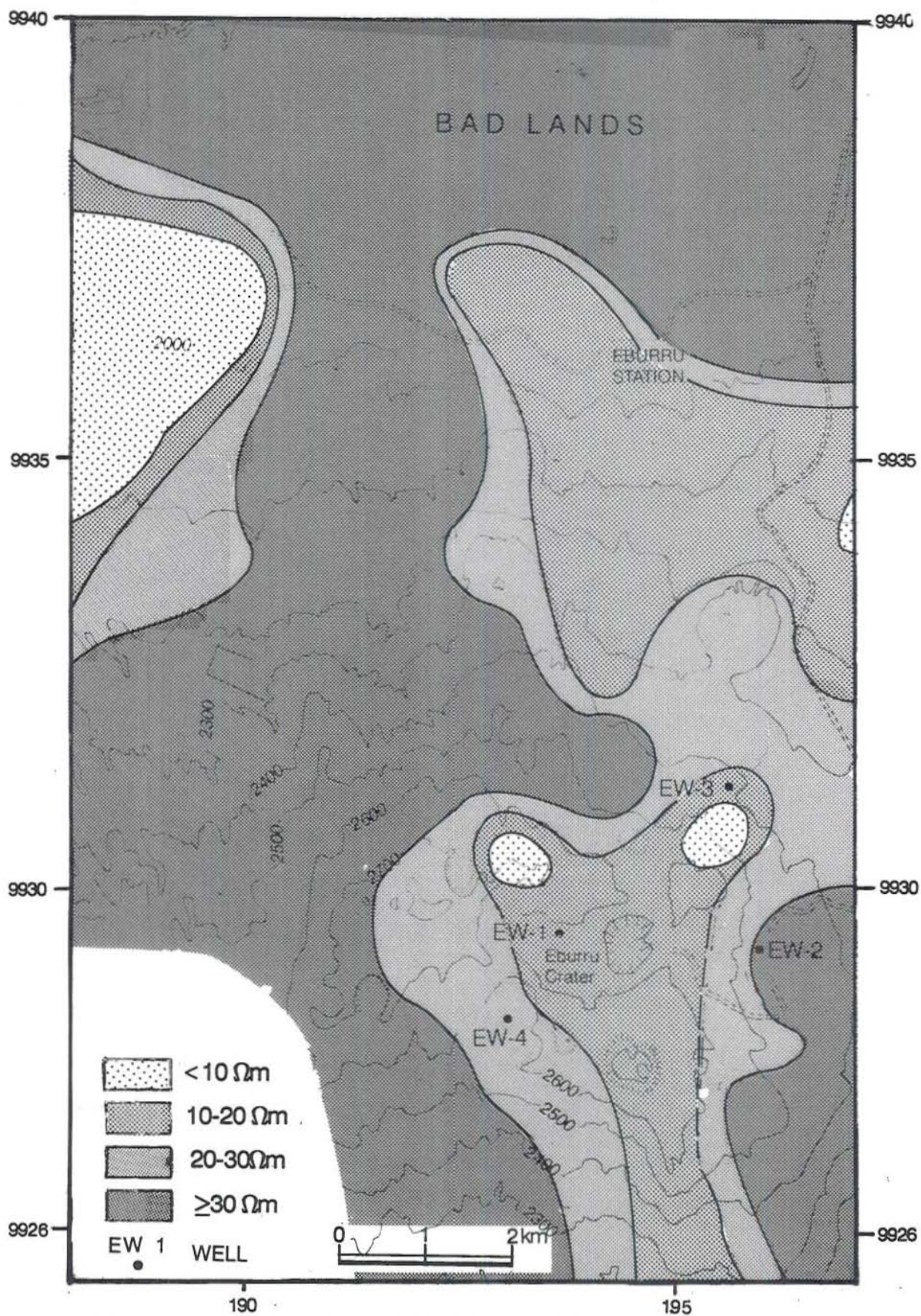
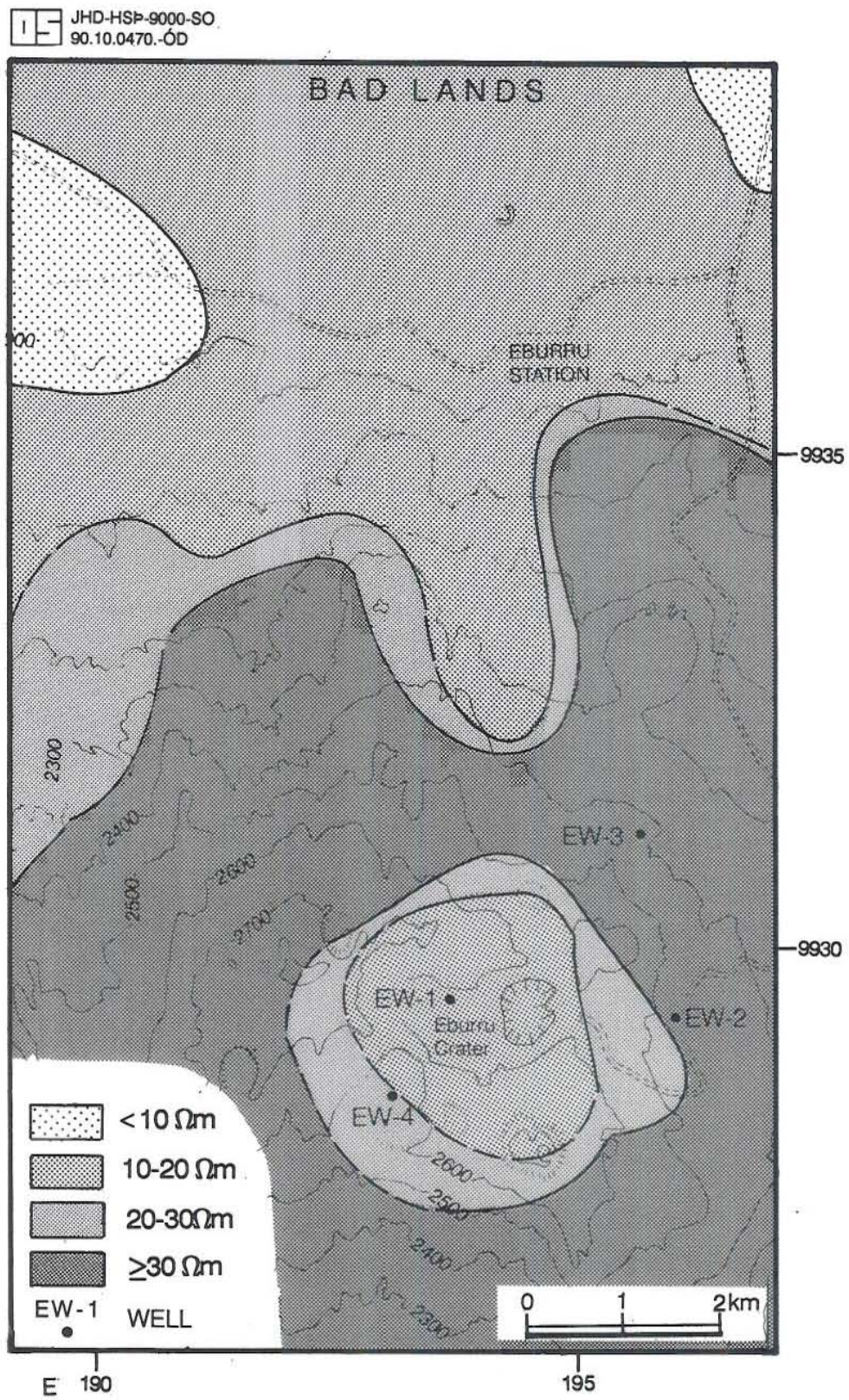FIGURE 8: Resistivity map of the Eburru-Badlands area at 1800 m a.s.l.

18

FIGURE 9: Resistivity map of the Eburru-Badlands area at 1000 m a.s.l.

2.5 Discussions

The combined results of 1-D and 2-D modelling may be related to permeability, degree of hydrothermal alteration and type of fluid in the rocks, and to the geological, structural and tectonic features of this area.

The resistivity structure agrees with some of the results from the drilled wells in the Eburru area. The high resistivity values at depth around Eburru correlate with low permeability, hydrothermal alteration and low measured temperatures, e.g. wells EW2, EW3, and EW4. The higher resistivity also correlates with the occurrence of a syenitic intrusion at depth (Figure 11). Gravity measurements (Simiyu, 1990) also give evidence of the intrusive body (Figure 12). The top of this intrusion is at about 1600 m a.s.l. to the north of the crater area. The resistive structure indicates that the crater anomaly is separated from the Badlands anomaly by a zone of low permeability and temperature. The Badlands anomaly has the same resistivity structure as the Eburru crater anomaly and this may suggest similar reservoir conditions. However, the lower resistivity below 1000 m a.s.l. in the Badlands area, might be an indication of either higher temperature or permeability.

The 20 - 100 Ωm layers at depth represent areas of temperatures between 50° - 150°C depending on the permeability distribution and degree of hydrothermal alteration. The lower temperatures at depth encountered in wells EW2, EW3 and EW4 are within these areas of higher resistivity. The 10 - 20 Ωm layer near the surface may be influenced by hydrothermal alteration of pyroclastics to low temperature clays (e.g. smectites). Fumaroles are also found where this layer comes close to the surface.

The sparse occurrence of fumaroles in the Badlands area may be due to the thicker high resistivity layer on the surface. The northward extension of the 10 - 20 Ωm layer (Figure 8) may be due to lateral flows from both the Eburru crater and Badlands anomalies through N-S trending fractures. The occurrence of this layer at deeper levels between EB54 and EB102 and around the Eburru station may indicate deeper percolation of 50° - 150°C geothermal fluids in E-W trending structures. The discontinuity around Eburru station has been observed in a previous resistivity interpretation (Onacha, 1990) and in gravity mapping (Figure 12).

The low resistivity in the crater area correlates with the effect of high salinity (fluid resistivity 2 Ωm) and high temperature (>200°C) below 1000 m a.s.l. This high temperature occurs in a narrow conduit which implies that the reservoir is largely controlled by vertical permeability, and fracture porosity is important. The resistivity anomaly indicates higher temperature closer to the surface to the north of well EW1. There are also near-surface outflows to the northwest, northeast and south (Figure 8). The outflows are mainly fault controlled (Figure 13). The northeast outflow passes through well EW3. It is also worth noting that the shape of the geochemistry anomaly coincides with the outflow paths of geothermal fluids and also the low resistivity anomaly (at 1000 m a.s.l.) seems to define the 200°C isotherm confined to the crater area within the proposed ring structure (see Figure 2).

Although the 2-D modelling has helped to define the north and south boundaries, their exact locations are not very well defined, due to the sparse data coverage. A clearer picture would be obtained if 2-D modelling of most of the soundings was carried out, augmented by the MT data to give a better resolution of deeper structures. The 2-D modelling of narrow low resistivity anomalies reduces the low resistivity values obtained from 1-D interpretation by a factor of more than two. The Badlands-Oljarai anomalies should be investigated further. The gravity high in this area is probably associated with the heat source, and the low resistivity (found in gravity lows) may relate to high permeability.

FIGURE 10: 2-D resistivity section along profile AB in the Eburru-Badlands area
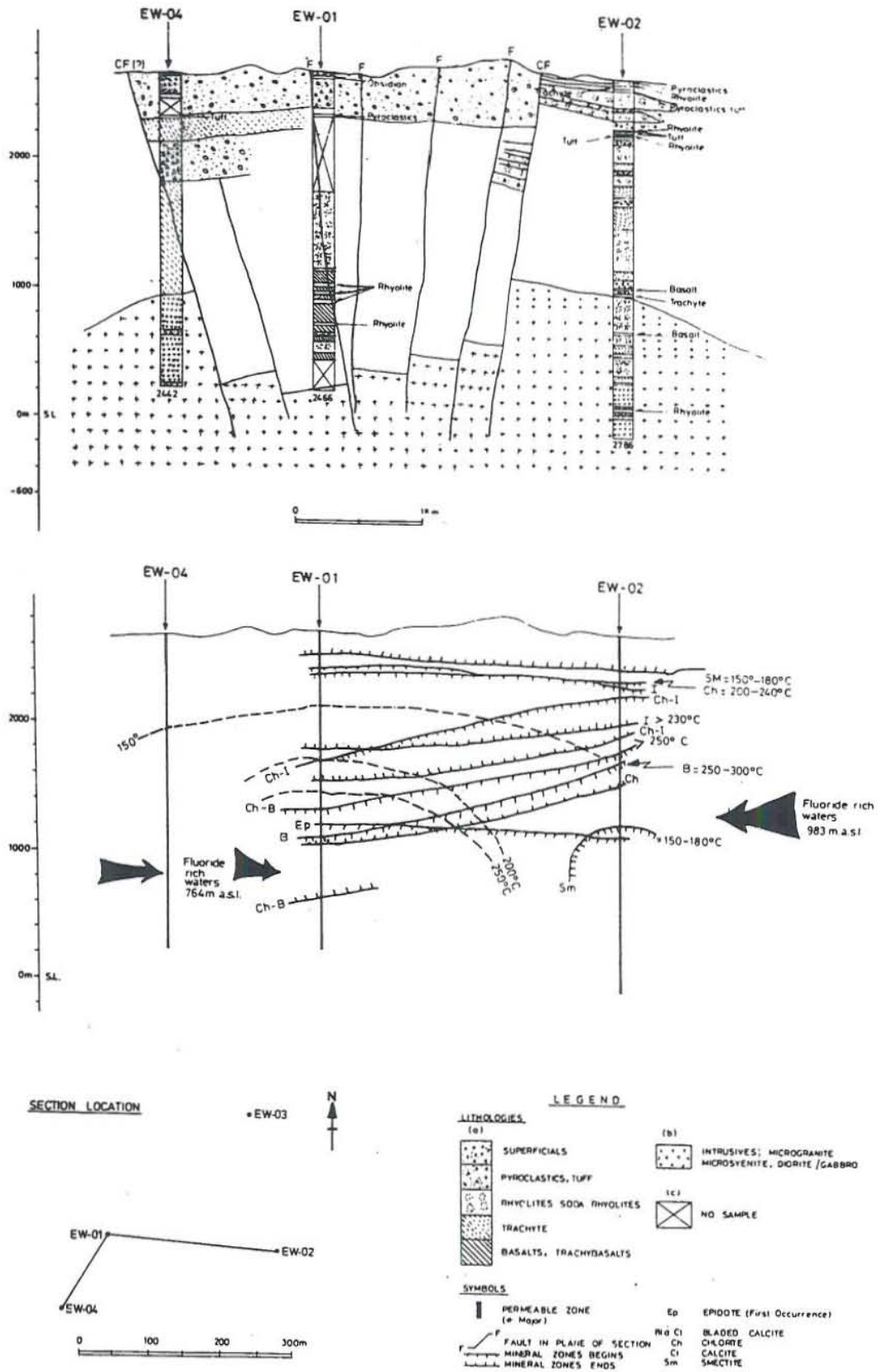
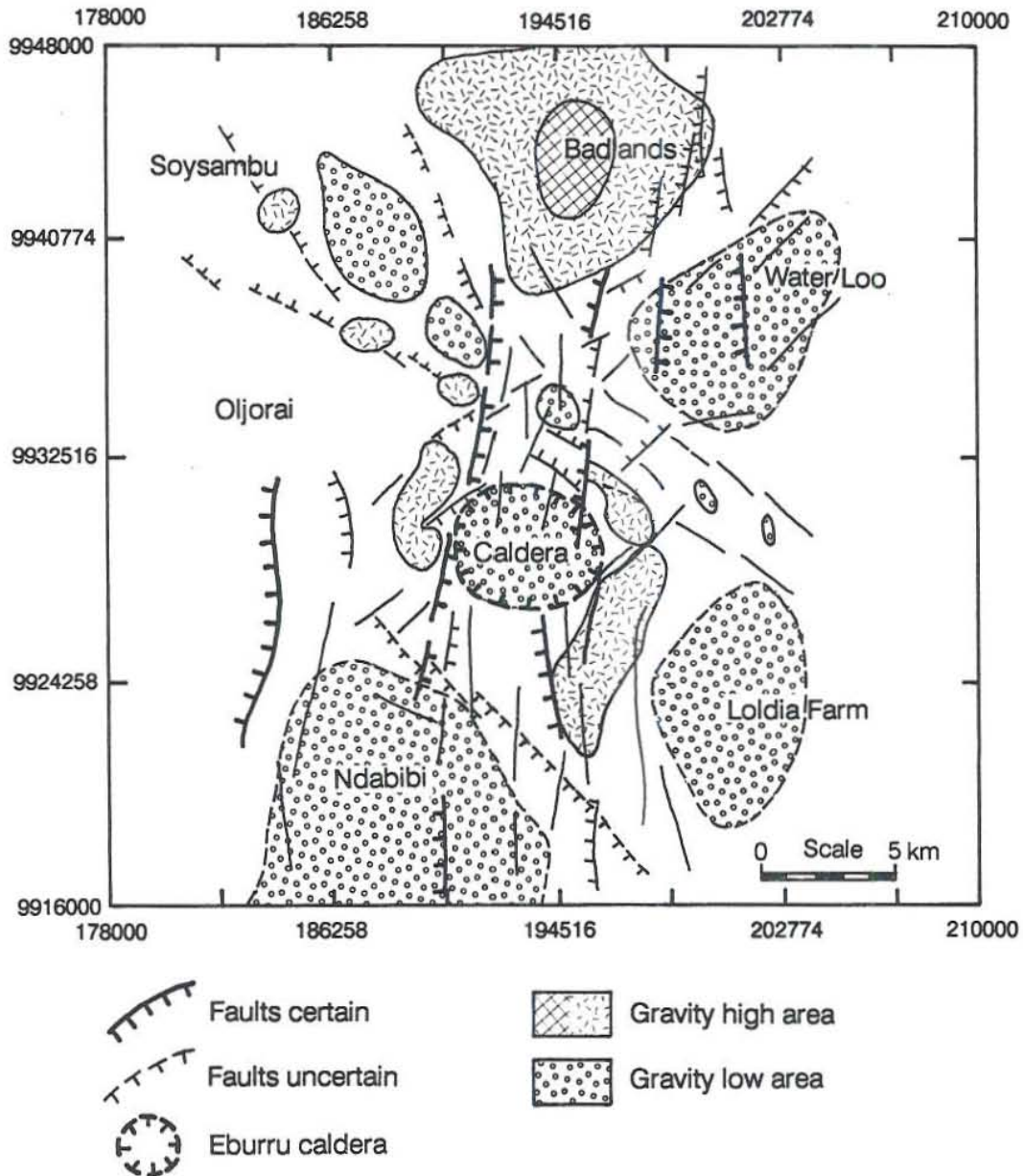FIGURE 11: Geological logs for wells EW1, EW2, and EW4 (Muchemi, 1990)

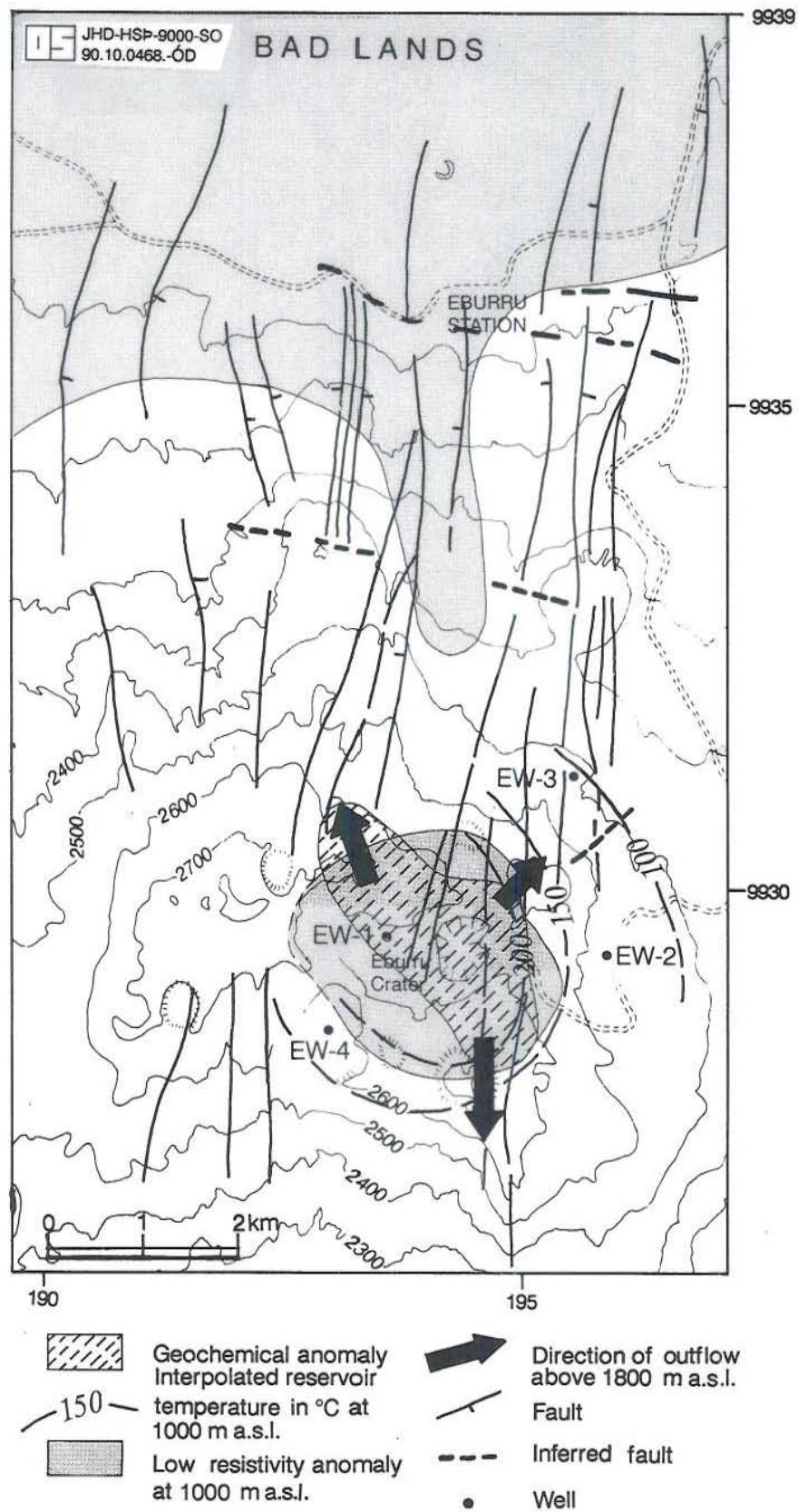FIGURE 12: Gravity structural map of the Eburru-Badlands area (Simiyu, 1990)

FIGURE 13: Resistivity, geochemical and structural anomalies in the Eburru-Badlands area

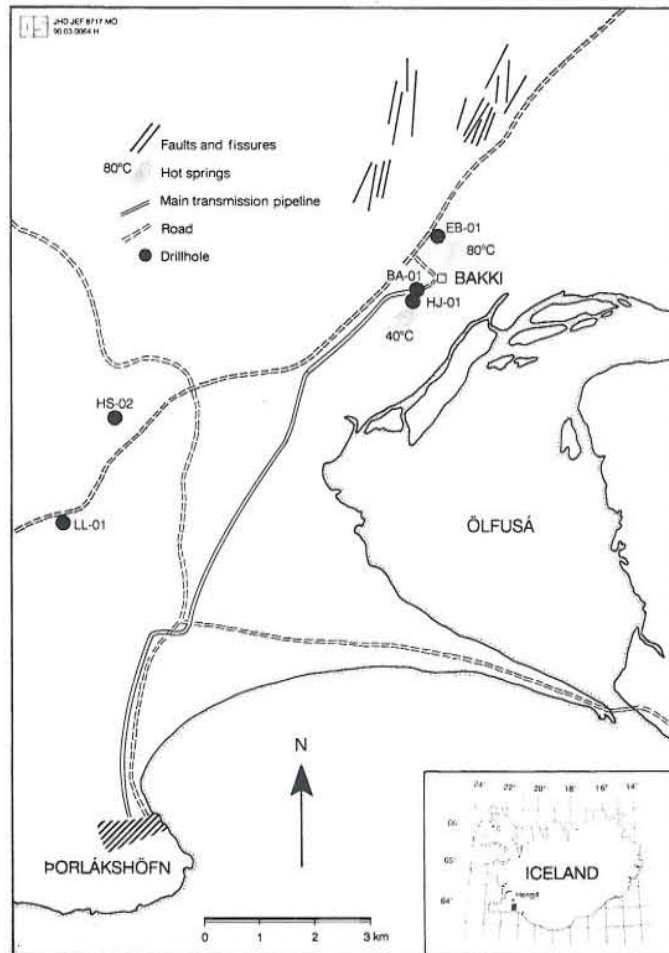# 3. TEM AND AMT/MT METHODS AT BAKKI, S-ICELAND

3.1 Introduction

FIGURE 14: Location of the Bakki geothermal field in the Olfus region of S-Iceland

The Bakki geothermal field is located in the Olfus region of the southern lowlands of Iceland (Figure 14). The active volcanic zone is to the west of this region . The area is mainly covered by basaltic hyaloclastites and clastic sediments of young Quaternary age. There have been repeated transgressions by the sea so that reservoir rocks have high salinity. The lithological logs from the production wells at Bakki indicate that formations are made of intercalations of tuffs, fine to medium grained fresh and altered basalts and fine to coarse grained sediments. The Bakki field has been exploited for the municipal heating system for the town of Thorlakshofn since 1979. The geothermal water is also utilized for fish farming.

The interpretation of Schlumberger and TEM soundings indicates that there is an extensive area of low resistivity (5-10) Ωm at 800 m b.s.l. (Figure 15). Probably the area enclosed by the 5 Ωm contour line (Georgsson, 1989) defines the boundaries of the field.

Geochemical measurements and temperature logs indicate that well HJ-01 has cooled by 5° to 6°C (Kristmannsdottir et al., 1990). The cooling has occurred in the deepest aquifers at a depth of 450 to 590 m. The cooling has been attributed to an inflow of cold groundwater through a fracture or fracture system in direct connection to the reservoir feeding the bottom aquifer.

3.2. TEM method

3.2.1. Introduction

The method used in the present study is the Central Loop Transient Electromagnetic sounding (CLTEM). In this method, a loop of wire is placed on the ground and a step current transmitted through it. When this current is turned off, an electric current is induced into the ground by the decaying magnetic field. The receiver coil is placed at the centre of the loop and the decay rate of the secondary magnetic field recorded as a function of time. The decay rate depends on the
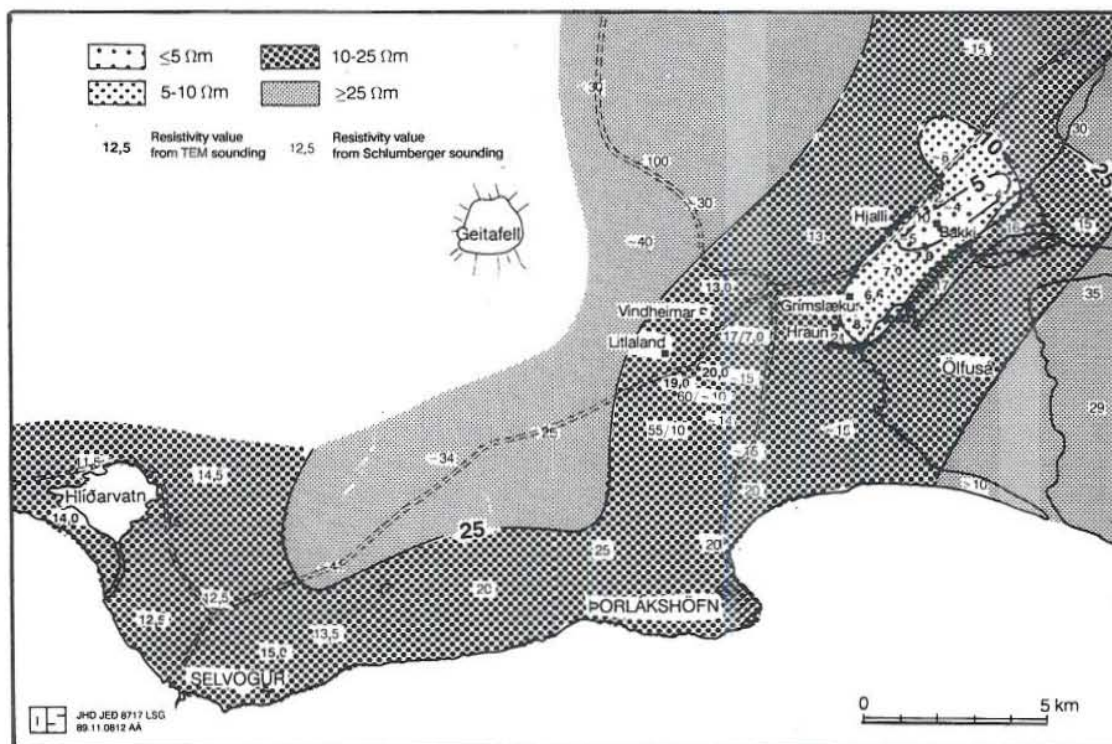
FIGURE 15:   Resistivity in the Olfus region at 800 m b.s.l. (Georgsson, 1990)

resistivity structure and may be used to evaluate the sub-surface resistivity structures. The depth of penetration depends on how long the induction in the receiver may be traced in time, which in turn is dependent on the effective areas of the receiver and transmitter coils, transmitted current and the resistivity structure.

The CLTEM method has several advantages over the DC sounding method. There is no direct injection of current into the ground, so that the transmitter only couples inductively to the ground. The method is less dependent on local resistivity inhomogeneities. The curves only respond to the surface inhomogeneity at early times. This is an important characteristic that may be applied to correcting static shifts in MT soundings (Sternberg et al., 1988). The method gives a stronger signal in low resistivity areas and is much faster and requires comparatively less manpower.

Although the theoretical treatment of the data interpretation procedures is more complicated than for DC sounding, 1-D interpretation is a better approximation of sub-surface resistivity. The method has been used successfully at several places in Iceland, and in the Asal Rift in Djibouti where it was used to map the saline groundwater table, and a geothermal system. An exhaustive treatment of the theory of this method is beyond the scope of the present study.

3.2.2. Overview of theory

The mathematical and physical basis of the TEM method is described in numerous publications (e.g. Kaufman and Keller, 1983; Ward and Hohman, 1988; Arnason, 1989). The interpretation of the response for 3-D structures has been outlined by various authors (e.g. McNeill et al., 1984; Newman et al., 1987).

The theory of the CLTEM in the case of a horizontally layered earth is based on Maxwell's equations for the electromagnetic field caused by a vertical magnetic dipole at the surface. By

using a magnetic vector and scalar potentials A and Φ, we get

$$\bar{E} = \bar{\nabla} \times \bar{A}, \qquad \bar{H} = \sigma \bar{A} + \epsilon(\partial \bar{A} / \partial t) - \bar{\nabla} . \Phi, \tag{3.1}$$

where $\bar{E}$ is the electric field intensity, $\bar{H}$ is the magnetic field intensity, μ is the permeability, and ϵ is dielectric permittivity. By imposing the gauge condition $\bar{\nabla}.\bar{A} = \mu \, \partial\Phi /\partial t$, it can be shown that

$$\nabla^2 \bar{A} - \mu\sigma \, \partial\bar{A} / \partial t - \mu\epsilon \, \partial^2\bar{A} / \partial t^2 = \mu \, \partial\bar{M} / \partial t. \tag{3.2}$$

$\bar{M}$ is the magnetic source dipole moment and is non-zero only at one point at the surface. Equation 3.2 is a dynamic equation that may be solved by imposing boundary conditions for the electromagnetic field at the interfaces between layers and at the surface (see Arnason, 1989). For harmonic time variation of the source dipole ($\bar{M} = M_0 \hat{z} e^{i\omega t}$), the azimuth component of the electric field at the surface of a homogeneous half-space can, in the quasi-stationary approximation, be expressed in the following analytical form:

$$E_\psi (r) = [-i\omega\mu_0 M_o / 2\pi] \ [(3 + 3ik^2r - k^2r^2) \ e^{-ik \, r} - 3] /k^2r^4, \tag{3.3}$$

where r is the distance along the surface from the source dipole to the measuring point.

The electrical field generated by the magnetic dipole without the earth can be written as:

$$E^o_\psi(r) = -i\omega\mu_0 M_o / 4\pi \, r^2. \tag{3.4}$$

The electrical field at the surface of a homogeneous half-space in the quasi-stationary approximation can, therefore, be written as:

$$E_\psi(r) = E^0_\psi(r) \, E^e_h(r), \tag{3.5}$$

where $\quad E^e_h(r) = 2 \ [(3 + 3ikr - k^2r^2)e^{-ikr} - 3] / k^2r^2. \tag{3.6}$

Similarly, at the surface of a horizontally layered earth:

$$E_\psi(r) = E^o_\psi(r) \, E^e(r), \tag{3.7}$$

where $E^e(r) = 2r^2 \ \int_0^\infty \lambda[S_0/(S_0 - T_0)] \, J_1 \, (\lambda r) d\lambda. \tag{3.8}$

The functions $S_0(\lambda)$ and $T_0(\lambda)$ are determined recursively in terms of frequency, resistivity, and thickness of successive layers. J_1 is the first order Bessel function.

The voltage measured in a receiver loop of radius r with the source dipole at the centre may be expressed as:

$$V = 2 \pi r \ n_r \, E_\psi(r) = A_r n_r \, 2E_\psi(r) / r, \tag{3.9}$$

$A_r = \pi r^2$, n_r = number of windings in the loop.

By using Equations 3.5, 3.8 and 3.9,

$$V(\omega,r) = A_r n_r \ A_s n_s I_o \, (-i \, \mu_0\omega) / \pi r \ \int_0^\infty \lambda \ [S_0/(S_0 - T_0)] \, J_1(\lambda r) d\lambda, \tag{3.10}$$

where we have written

$$M_0 = A_s n_s I_0.$$

By the principal of reciprocity, the source and receiver may be interchanged. Therefore, Equation 3.10 also describes the voltage generated in a receiver coil of effective area A_s n_s at the centre of a source loop of effective area A_r n_r.

The transmitted current is usually a square wave such that the abrupt change when current is turned off, may be treated as an individual step function. The induced voltage can, in this case, be shown to be given by a cosine transform integral as a function of time.

$$V(t,r) = 2/\pi \int_0^\infty Re[V(\omega,r) / -i\omega] \cos(\omega t) \, d\omega. \tag{3.11}$$

The integrals in Equations 3.10 and 3.11 may be expressed as a convolution integral by changing to logarithmic variables. The convolution can be evaluated by digital filters (Arnason, 1989). The induced current distribution after current turnoff may be viewed as a diffuse current ring which propagates downwards and outwards from the source loop (Nabighian, 1979; Hoversten and Morrison, 1982). If the series expansion of e^{-ikr} is applied to Equation 3.6, the induced voltage can be shown to be given as:

$$V(r,t) \approx [C/10\pi^{1/2} \ (\mu_0 \ \sigma \ r^2)^{2/3}] / t^{5/2} \quad \text{for large t,} \tag{3.12}$$

where $C = [A_r \ n_r \ A_s \ n_s \ \mu_0]/2\pi r^3$.

Hence, the late time apparent resistivity is defined by:

$$\rho_a(r,t) = (\mu_0 / 4\pi) \ [(2\mu_0 A_r n_r A_s n_s) / (5t^{5/2} \ V_c(r,t))]^{2/3}. \tag{3.13}$$

The results of CLTEM soundings are usually expressed in this form.

3.2.3 Data acquisition and analysis

The author took part in data acquisition of 5 TEM-soundings (AÖ17 - AÖ21) (for location, see Figure 16). The field equipment consisted of a transmitter, receiver, generator, and receiver and transmitter loops. The receiver loops consisted of a small coil with an effective area of 100 m^2 and a flexible loop with an effective area of 8112 m^2. Square transmitter loops of side length of 200 - 300 m were used. The transmitter and receiver are synchronized through crystal clocks and the data are digitally recorded as voltage versus time in the receiver. The current turn-off time which is dependent on the size of the transmitter loop, was also recorded. The data was recorded over high and low frequency sweeps.

Preliminary data analysis includes stacking of the recorded voltages. The stacked data is edited to remove any spurious measurements due to cultural noise and then the results averaged to obtain induced voltages as a function of time. The voltage values are converted to apparent resistivity as a function of time by use of Equation 3.13.

One-dimensional interpretation of the smoothed data was carried out using an iterative Levenberg-Marquardt type inversion. The goal was to determine the layered earth model whose response produces the measured values as closely as possible. The data and the model curves are presented in Appendix B.
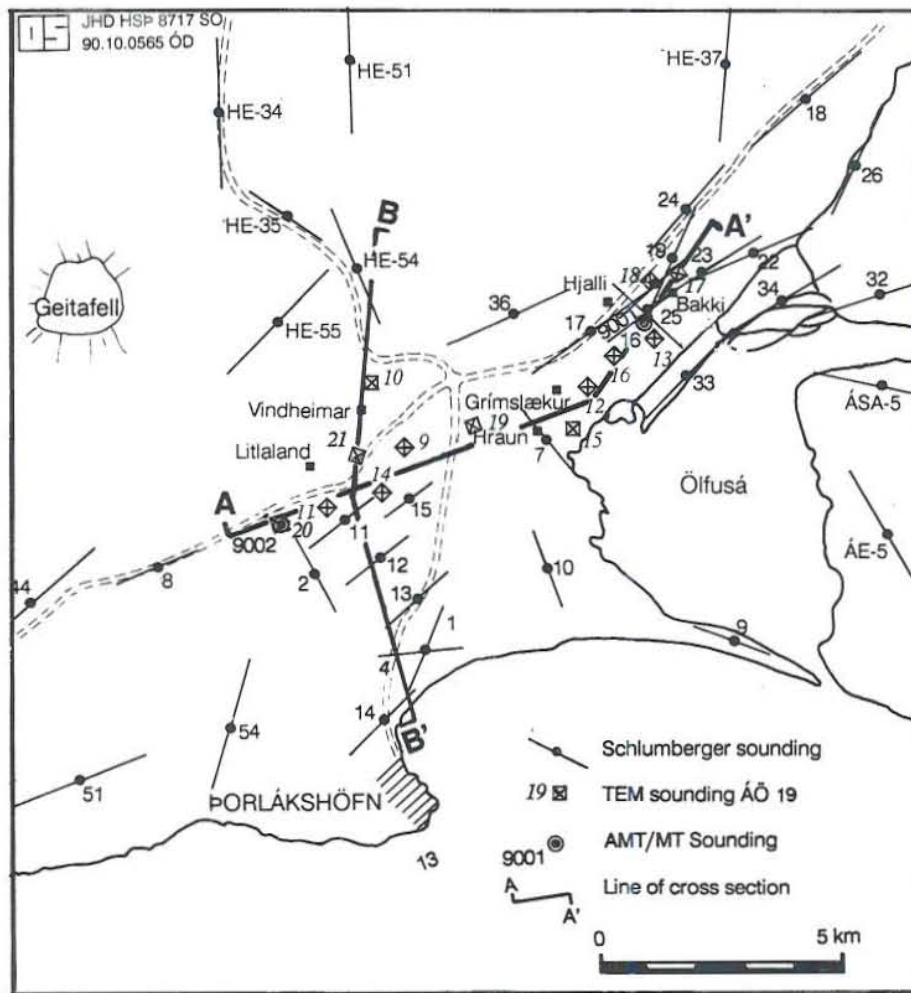
FIGURE 16: Location of DC Schlumberger, TEM and AMT/MT soundings in Olfus

3.2.4 Interpretation of the results

The results were incorporated into the previous interpretation by Georgsson (1989). Two profiles, AA' and BB' are presented. The location of the profiles is shown on Figure 16. Profile AA' (Figure 17) is represented by a five layer model. The first surface layer has high resistivity ($\geq$ 500 Ωm) and the thickness varies between 30 - 80 m. This layer is not found between Grimslaekur and Bakki. The second layer (30 - 100 Ωm) is at the surface in the vicinity of Bakki, it dips to the southwest and its thickness ranges from 50 - 100 m. The third layer (10 - 30 Ωm) dips to the southwest and has a thickness of 100 - 200 m. The fourth layer has the lowest resistivity ($\leq$ 10 Ωm) and has a thickness of 250 - 600 m. The bottom section shows indications of higher resistivity but the values are poorly defined. Evidence from AMT/MT (section 3.3.4) shows that this layer is very thick and has resistivity of > 30 Ωm.

Profile BB' (Figure 18) combines TEM and Schlumberger soundings. This profile shows the same features as profile AA'. The main difference is the discontinuity of the low resistivity layer ($\leq$ 10 Ωm) between AÖ10 and AÖ21. This implies that the low resistivity layer is either deeper or absent to the north around Vindheimar. The exact location of this discontinuity is not well defined. The low resistivity layer towards Thorlakshofn is not resolved by the DC soundings.

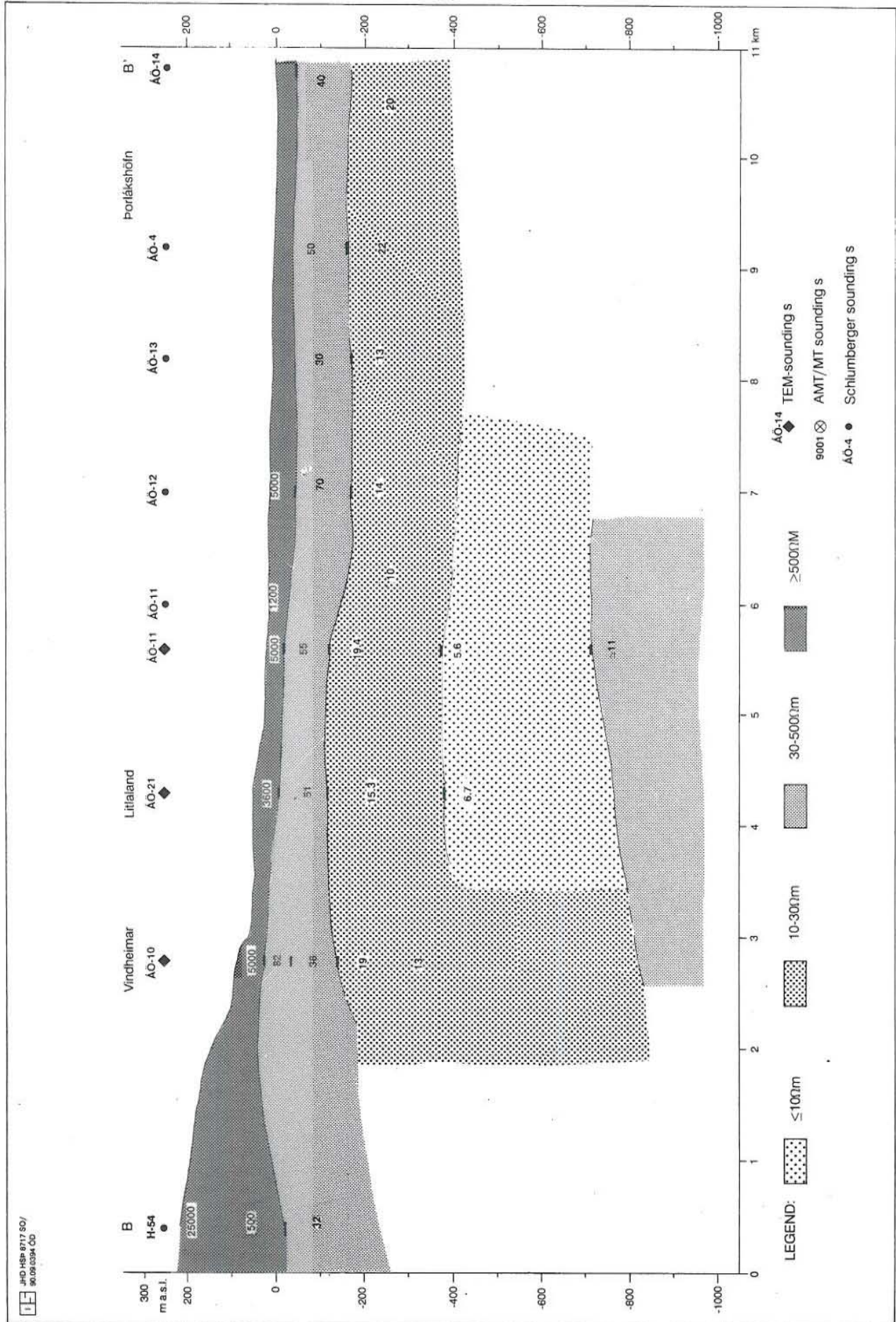FIGURE 17: 1-D TEM resistivity section along profile AA' from Hlidarendi to Bakki
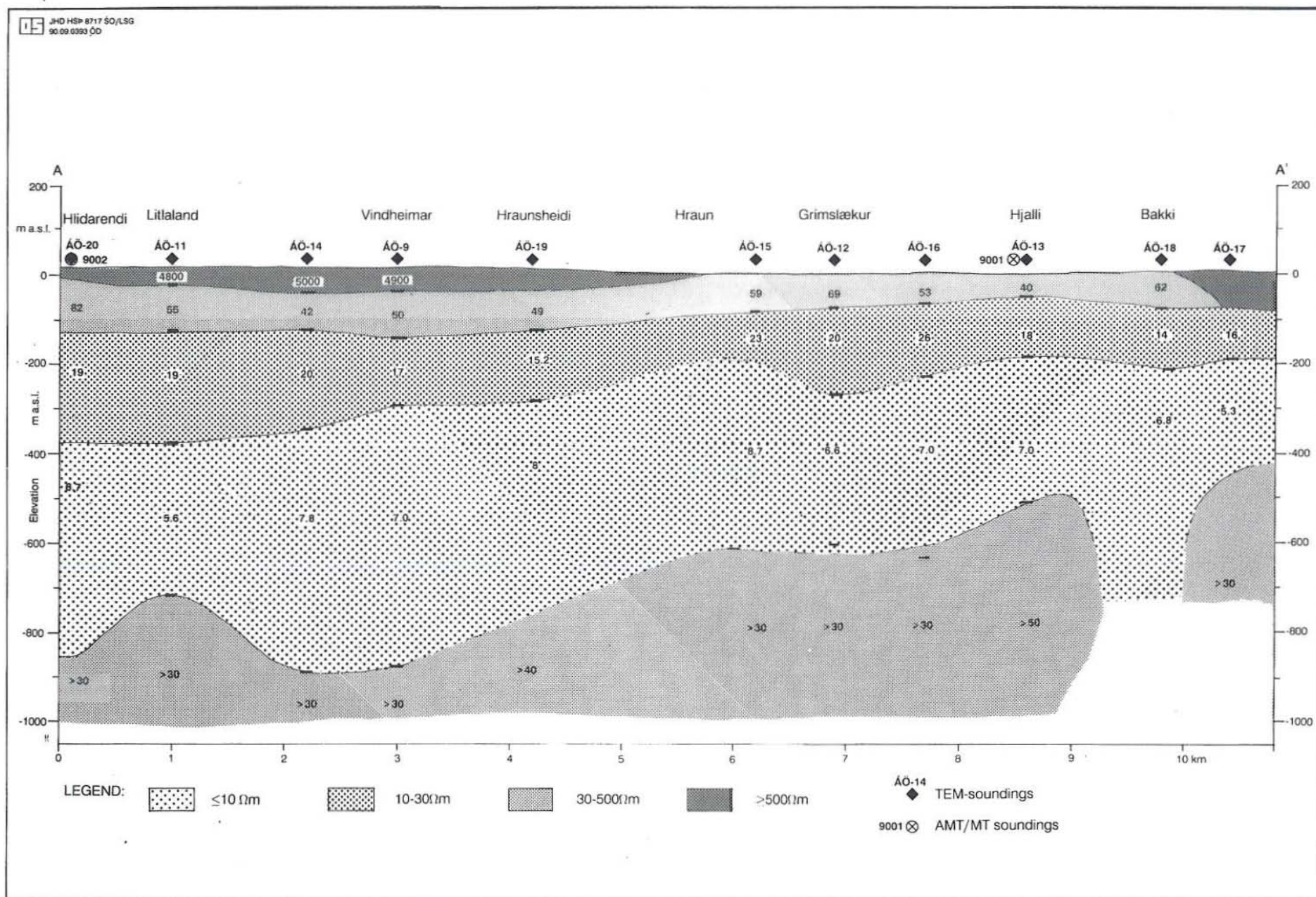
FIGURE 18: 1-D TEM and DC Schlumberger resistivity section
along profile BB' from Vindheimar to Thorlakshofn

3.3 Audiomagnetotelluric (AMT) and magnetotelluric (MT) methods

3.3.1 Introduction

The two methods are the same in application. The only difference is the frequency range, i.e 0.1 to 10^4 Hz for AMT and 10^{-4} to 10 Hz for MT. The electrical properties of the subsurface are determined from the measurements of orthogonal components of the natural time varying electrical and magnetic fields. The electrical fields are detected between orthogonal sets of non-polarizing electrodes while the magnetic fields are detected by induction coils, squids, or fluxgate magnetometers. The data acquisition procedures are more or less the same where either two or three components of the magnetic field and two components of the electrical field are measured. The orthogonal electrical and magnetic fields are related through the impedance tensor.

3.3.2 Theory

The detailed development of the theory of this method may be found in various publications, e.g Vozoff (1972), Kaufman and Keller, (1981) and Ward and Wannamaker (1983), upon which this overview is based. The 1-D formulation is developed from Maxwell's equations assuming an incidental plane wave and no displacement currents. The relation between the orthogonal electrical and magnetic fields is given by:

$$Z_{xy} = E_x/H_y = i \mu_0\omega / k, \tag{3.14}$$

$$Z_{yx} = E_y/H_x = -i \mu_0\omega / k, \tag{3.15}$$

where Z_{xy} and Z_{yx} are the impedance ($Z_{xy} = - Z_{yx}$), x and y are measuring directions, ω is the angular frequency, μ_0 is the magnetic permeability, and $k^2 = i\mu\omega / \rho$. The apparent resistivity ρ_a can be calculated from Equation 3.14 or 3.15 as:

$$\rho_a = (1 / \omega\mu) |Z_{xy}|^2 = (1 / \omega\mu) |Z_{yx}|^2. \tag{3.16}$$

Equation 3.16 can also be written as:

$$\rho_a = 0.2 T | Z |^2, \tag{3.17}$$

where Z ($= Z_{xy}$ or Z_{yx}) is in (mV/km)/gamma, and T is the period in seconds.

The skin depth δ is defined as the depth when the fields have reduced to e^{-1} of their surface values and is given by:

$$\delta = \text{Real} (1/k) = (T\rho/2\pi\mu)^{1/2} \approx 0.5 (T\rho)^{1/2} \text{ km.} \tag{3.18}$$

For an N - layered earth, the plane wave impedance is given by a recursive formula (Ward and Wannamaker, 1983):

$$Z\check{}_{n-1} = Z_{n-1} [Z\check{}_n + Z_{n-1} \tanh(ik_{n-1}h_{n-1})] / [Z_{n-1} + Z\check{}_n \tanh(ik_{n-1}h_{n-1})], \tag{3.19}$$

where

$Z_n = \mu_0\omega/k_n$ (intrinsic impedance of nth layer),
$Z\check{}_n =$ impedance at the top of the nth layer,

k_n and h_n are the wave number and thickness of the nth layer respectively, and $Z^{\sim}_N = Z_N$.

In the 2-D case, the resistivity is invariant in one direction. This axis, along which there is no variation in resistivity, is known as the strike direction. The electrical and magnetic fields are related through the impedance tensor. In the E-polarization (T_E mode), the electrical field is parallel to the strike and in the H-polarization (T_M mode), the electrical field is perpendicular to the strike. If x' is the strike direction, then

$$Z_{xy} = E_{x'}/H_{y'} = Z_{TE}, \tag{3.20}$$

$$Z_{yx} = E_{y'}/H_{x'} = Z_{TM}. \tag{3.21}$$

In matrix notation

$$\bar{E} = \begin{bmatrix} E_{x'} \\ E_{y'} \end{bmatrix} = \begin{bmatrix} O & Z_{xy} \\ Z_{yx} & O \end{bmatrix} \begin{bmatrix} H_{x'} \\ H_{y'} \end{bmatrix} = [Z]\,\bar{H}. \tag{3.22}$$

If measurements are made in any arbitrary directions, we may rotate them to find the direction of strike x' by minimizing diagonal elements (or maximizing the off-diagonal elements of the tensor). The principle direction for clockwise rotation is defined below by maximizing

$$|Z_{xy}(\Theta)|^2 + |Z_{yx}(\Theta)|^2, \tag{3.23}$$

and $$\tan(4\Theta_0) = \frac{(Z_{xx} - Z_{yy})(Z_{xy} + Z_{yx})^* + (Z_{xx} + Z_{yy})^*(Z_{xy} - Z_{yx})}{|Z_{xx} - Z_{yy}|^2 - |Z_{xy} + Z_{yx}|^2}, \tag{3.24}$$

where * is the complex conjugate and Θ_0 (or $\Theta_0 + 90°$) is called the principle direction.

The tipper (T) is given by:

$$T = [\,|A|^2 + |B|^2\,]^{1/2} \text{ where } H_z = AH_x + BH_y. \tag{3.25}$$

If x is the strike direction, then for the T_M mode there is no H_z, and A reduces to zero. Thus, the tipper can be used to determine the strike direction.

The skew (S) defined below is a measure of dimensionality and large skew (≥ 0.4) implies 3-D (Vozoff, 1972),

$$S = \frac{|Z_{xx} + Z_{yy}|}{|Z_{xy} - Z_{yx}|} \tag{3.26}$$

The impedance tensor may be calculated in the least square fit by minimizing

$$F = |E - ZH|^2. \tag{3.27}$$

From Equation 3.22, we have in the measuring direction (x and y):

$$E_x = Z_{xx}H_x + Z_{xy}H_y, \tag{3.28}$$

$$E_y = Z_{yx}H_y + Z_{yy}H_y. \tag{3.29}$$

The least square fits (Ward and Wannamaker, 1983) give:

$$Z_{xx} = [(\overline{E_xH_x^*}) \, (\overline{H_yH_y^*}) - (\overline{E_xH_y^*}) \, (\overline{H_yH_x^*})] \, / \, D, \qquad (3.30)$$

$$Z_{xy} = [(\overline{E_xH_y^*}) \, (\overline{H_xH_x^*}) - (\overline{E_xH_x^*}) \, (\overline{H_xH_y^*})] \, / \, D,$$

$$Z_{yx} = [(\overline{E_yH_x^*}) \, (\overline{H_yH_y^*}) - (\overline{E_yH_y^*}) \, (\overline{H_yH_x^*})] \, / \, D,$$

$$Z_{yy} = [(\overline{E_yH_y^*}) \, (\overline{H_xH_x^*}) - (\overline{E_yH_x^*}) \, (\overline{H_xH_y^*})] \, / \, D,$$

where $D = (\overline{H_xH_x^*}) \, (\overline{H_yH_y^*}) - (\overline{H_xH_y^*}) \, (\overline{H_yH_x^*}).$

* denotes the complex conjugate and the bars indicate smooth auto and cross powers defined as:

$$\overline{A_iB_j} = \sum_{k_1}^{k_2} A_i^k B_j^k \, w^k. \qquad (3.31)$$

Where A and B are either E or H, i and j are either x or y and A^k is the kth fourier coefficient. The weighting function w^k is generally a Hamming window from f_1 to f_2 around the centre frequency f_0, where $f_1 < f_0 < f_2$ and $f_1 = k_1 \, / \, (N\Delta t)$, $f_2 = k_2 \, / \, (N\Delta t)$, Δt is the sampling interval and N is the number of samples.

Equations 3.28 and 3.29 may also be expressed as:

$$H_x = H_{xx}E_x + A_{xy}E_y, \qquad (3.32)$$

$$H_y = H_{yx}E_x + A_{yx}E_y,$$

$$\text{or} \quad \overline{H} = [A] \, \overline{E},$$

and A is known as the admittance tensor.

Aliasing is a problem encountered in data sampling. For a sampling interval of Δt the Nyquist frequency f_c is defined by $f_c = 1/ (2 \, \Delta t)$ such that frequencies above f_c are folded back into the range $0 - f_c$. All data with frequency $2nf_c + f$ have the same cosine function as that of frequency f sampled at $\Delta t = 1/ (2f_c)$. Therefore, a low pass filter with cut off frequency $\leq f_c$ is used before sampling (antialiasing filter).

If a time series $x_a(t)$ is sampled over the same time interval T such that

$$x(t) = x_a(t) \cdot d(t), \qquad (3.33)$$

where $\quad d(t) = \begin{cases} 0 & t < 0 \;\; t > T, \\ 1 & 0 < t < T \end{cases} \qquad (3.34)$

is called a boxcar window.

In the frequency domain, Equation 3.33 becomes a convolution of the form;

$$X(\omega) = X_a(\omega) * D(\omega),\tag{3.35}$$

where $D(\omega) = T\ [\sin\ \omega T/2]/\ \omega T/2.$ $\qquad\qquad\qquad\qquad\qquad\qquad\qquad\qquad$ (3.36)

For the time series with a single frequency ω_0, $x_a(t) = \sin\ \omega_0 t$,and the Fourier transform of $x_a(t)$ is a delta function $\delta(\omega - \omega_0)$. After convolution in the frequency domain, the final spectrum is different from the true spectrum. This is called leakage and is caused by energy from the existing frequency being leaked into the side lobes where no real power exists. The leakage can be reduced by applying windows with smaller side lobes, then the boxcar window e.g. the Hanning window, the Hamming window or the cosine taper window.

The most common inversion methods are the least square and the damped least square methods where the nonlinear MT response function is approximated by linearization using the Taylor series expansion of the MT response function about a starting model. The partial derivatives of the response function (i.e the Jakobian or the sensitivity matrix) can be calculated analytically for 1-D and 2-D inversion problems (Eysteinsson, 1988). In the damped least square method, the damping factor at each iteration is optimized to minimize the difference between the observations and model responses.

Generally, the E-polarization (T_E mode) apparent resistivity curve and the associated phase are utilized in 1-D modelling (Jones and Hutton, 1979). However, in the presence of 3-D structures, the use of either the invariant impedances (Ingham, 1988) or the determinant impedances (Ranganayaki, 1984) may be preferable.

The AMT/MT method is inherent with problems both in data acquisition and interpretation. The first problem is encountered in the source dimensions. Although the plane wave assumption is valid in the frequency range 10^{-4} - 1 Hz, significant errors may occur at frequencies less than 0.1 Hz in areas of high resistivity within 500 km of the position vertically above the electrojet (Bannister, 1969). Random equipment noise and quantization errors are frequently encountered on the magnetic channels due to the movement of magnetometers in the earth's magnetic field. Electromagnetic inductive noise occurs on both magnetic and electric channels. This noise comes from non-plane wave components of the electromagnetic field which may be either natural or manmade. Other sources of noise include geological noise due to the overburden or topography (Ku et al., 1973), current channelling (Jones, 1988), frequency-independent anisotropy (Ward and Wannamaker, 1983) and static shifts. These shifts are caused by shallow inhomogeneities that lead to a constant vertical displacement of the MT apparent resistivity curve on a log scale independent of frequency. Prior to inversion, one needs to shift the measured apparent resistivity by this constant factor.

The effects of noise on data may be reduced during data acquisition by remote reference (Clarke et al., 1983). The use of notch filters and delay time filters are appreciable (Fontes et al., 1987). Irregular coherent noise may be eliminated by the use of either the maximum entropy method, or window deconvolution techniques. Hattingh (1989) has proposed the use of the correlated data-adaptive noise cancelling method (CANC) to reduce the bias error, as well as random error, of the magnetotelluric impedance tensor.

3.3.3 Acquisition and analysis of AMT / MT field data from Bakki

Data acquisition was carried out at two sites. Both AMT and MT were measured at site 9001, but only AMT at 9002 (see Figure 16). The magnetic field was measured by two horizontal induction coils while the electrical fields were measured by a pair of non-polarizing copper sulphate electrodes placed at 100 m distance in the N-S and E-W directions. The AMT data was recorded over two overlapping bands of 0.05 to 5 and 0.5 to 50 s at 64 and 8 Hz sampling intervals respectively. The MT data was collected at 1 Hz sampling interval with a low pass filter at 0.3 Hz and no high pass filter.

The time series for 4096 samples in AMT and up to 32,768 in MT was plotted to check for any spurious data points. After detrending and tapering, the data was transformed to the frequency domain by the Fast Fourier Transform (FFT) and the impedance tensor determined by the eigenstate estimator. The data was evaluated further by considering the coherence in phase and resistivity, predictability, and skew at all frequencies. Predicability of higher than 0.8 and skew of less than 0.2 was used as the basis of data acceptance. The angle of fixed rotation was about 30° from the magnetic north over the whole frequency range for the two sites. The AMT / MT data is given in Appendix C. No quantitative analysis of the noise was carried out. The data indicates that the E and H polarization are affected by the ocean. The E polarization is biased down while the H polarization is biased up at low frequencies. A previous study of the ocean effect indicates that 10 km away from the coast (Figure 19), the effect is less than 6% for E polarization for periods less than 100 s (Eysteinsson and Hermance, 1985).
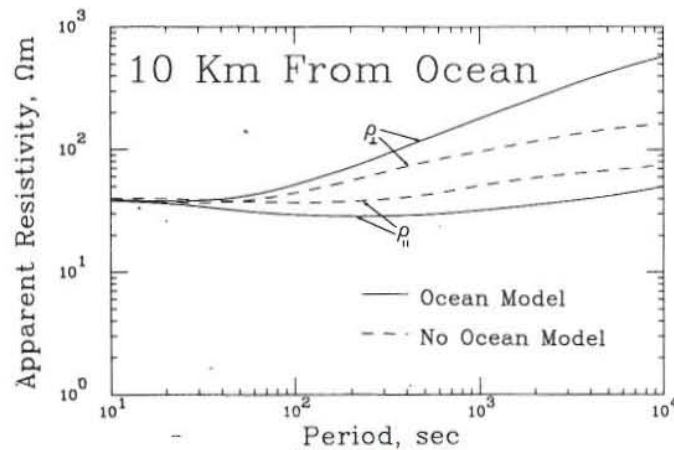

FIGURE 19:   Theoretical MT apparent resistivity curves, 10 km away from the ocean. The solid lines show the presence of the ocean while dashed lines indicate the absence of the ocean for both E and H polarization (Eysteinsson and Hermance, 1985)

The first step in the interpretation of the data was to determine the appropriate shift to be used to constrain the MT data to fit the TEM interpretation. Theoretical 1-D MT models were computed from TEM models at the two sites and compared with the measured MT data. The initial shift was then calculated from this comparison. Various models and shifts were then tried for the E polarization (yx), H polarization (xy), and the determinant resistivity estimates by using the TEM results to constrain the inversions. The principal directions are parallel to the Neovolcanic zone and the ocean but the strike direction cannot be determined. The present study assumes the direction of strike to be parallel to the coastline.

The root mean square error (Q) was used as a measure of the fit between the data and the model parameters. It was found that the E polarization gave models that were consistent with TEM results. The H polarization results gave higher resistivity and thickness values of the layers. It is noted that when constraining the model by the TEM results for the first km, there is an optimum shift for a good data fit; an increase or decrease of this optimum shift gives poorer data fit (Figure 20). For site 9002 the optimum shift was found to be 0.08, and 0.085 for site 9001. The inversion of unshifted data from site 9002 where we have constrained the model with the TEM results gives poor data fit as shown in Figure 21. Probably the best way of evaluating the shifts would be a joint MT and TEM inversion.
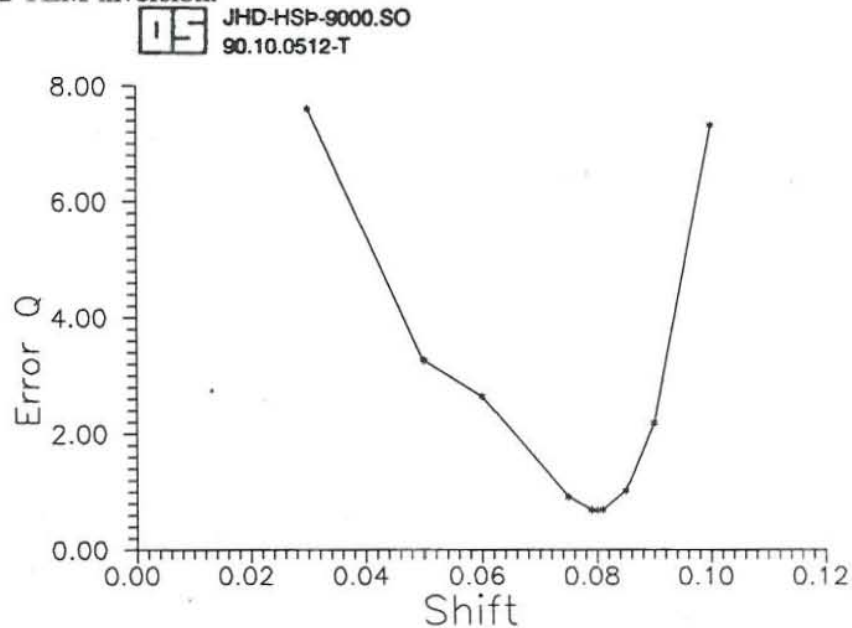
FIGURE 20: The effect of shift on the model response fit for MT data from site 9002 data
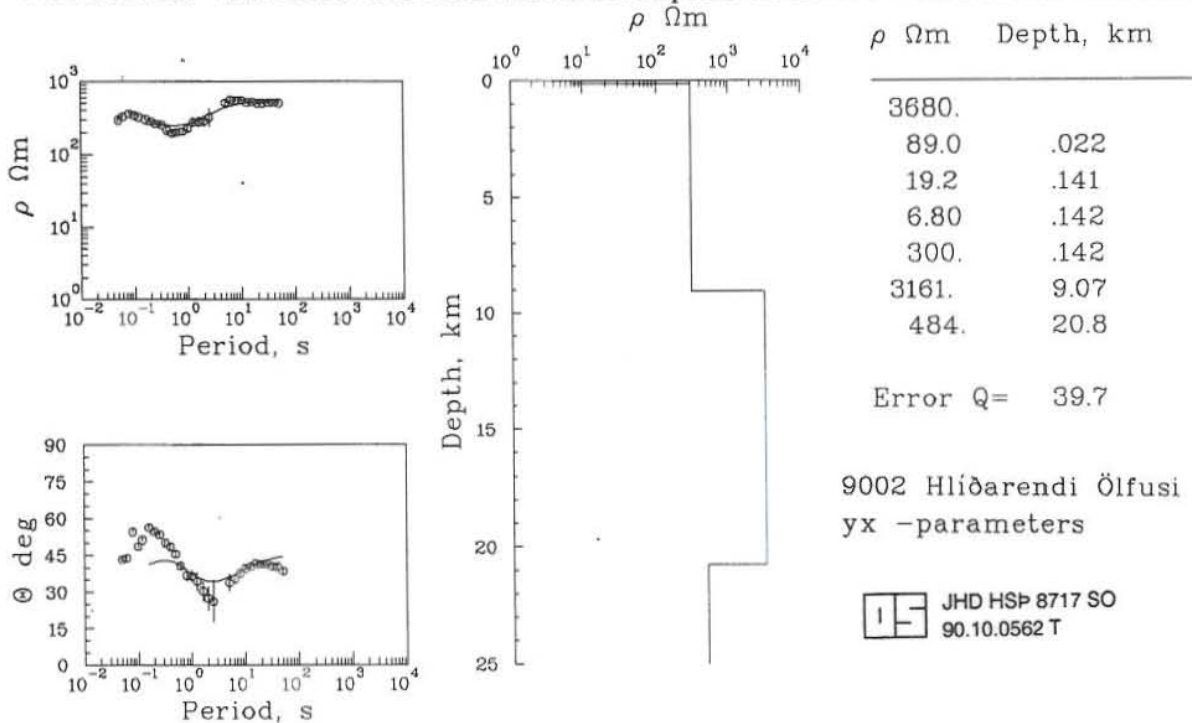
FIGURE 21: The inversion model of constrained and unshifted data for MT site 9002, showing poor data fit (direction of fixed rotation is 30°)

The inversion of the shifted data was carried out by the non-linear damped least square method. Seven layer models for the two sites (Figure 22) were found to represent the minimum number of layers that gave an adequate fit to the data. For site 9001, the resistivity of the first three layers and thicknesses of the first two layers were fixed from the TM results, while at site 9002, the resistivity of the first four layers and thicknesses of the first two layers were fixed.

3.3.4 Interpretation of the results

The interpretation of E polarization AMT/MT data as well as the results from the TEM soundings are shown on profile AA' (Figure 23) (see Figure 16 for location of the profile). The interpretation has given an indication of the thickness (250 - 600 m) of the low resistivity layer (<10 Ωm) within the uppermost kilometre. The results also show that there is a thick (>4 km) resistive layer (> 100 Ωm) below the surface low resistivity. A low resistivity (< 5 Ωm) layer is found at site 9001 near Bakki between 5 and 7 km. This layer is not resolved by the AMT data at Hlidarendi. The low resistivity layer may be related to the geothermal structure at Bakki. The very low resistivity at Bakki is underlain by higher resistivity at a depth of more than 7 km. However, more data is needed for a detailed interpretation.
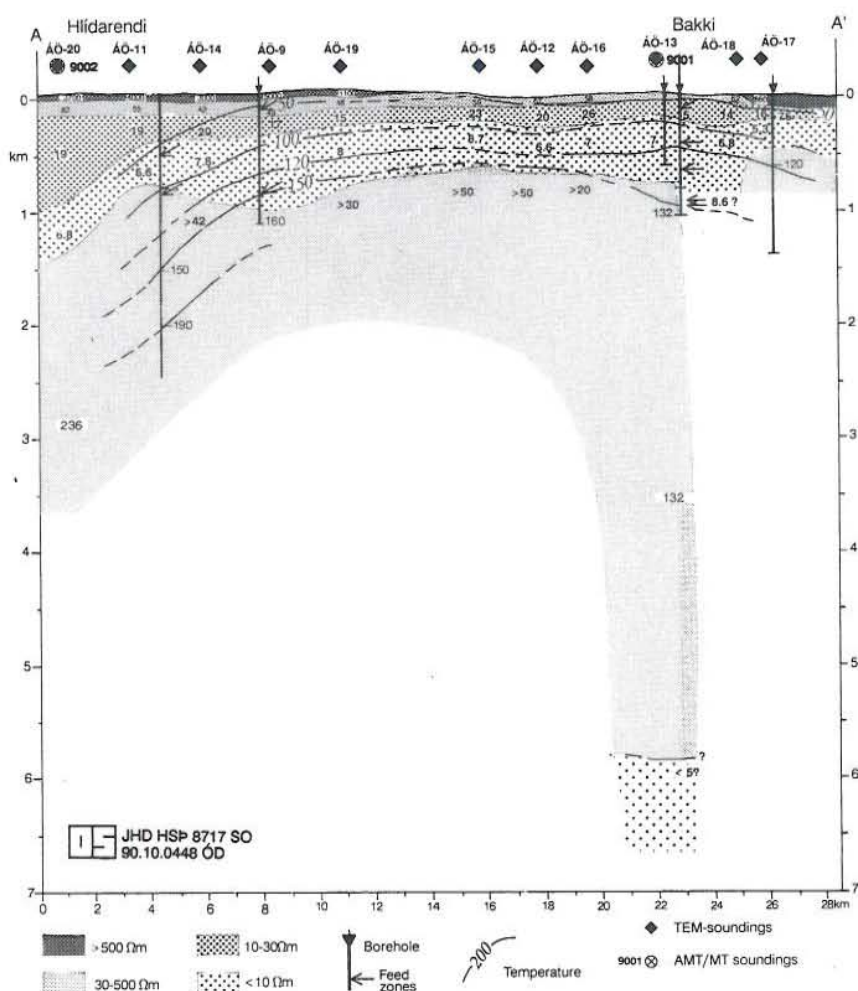

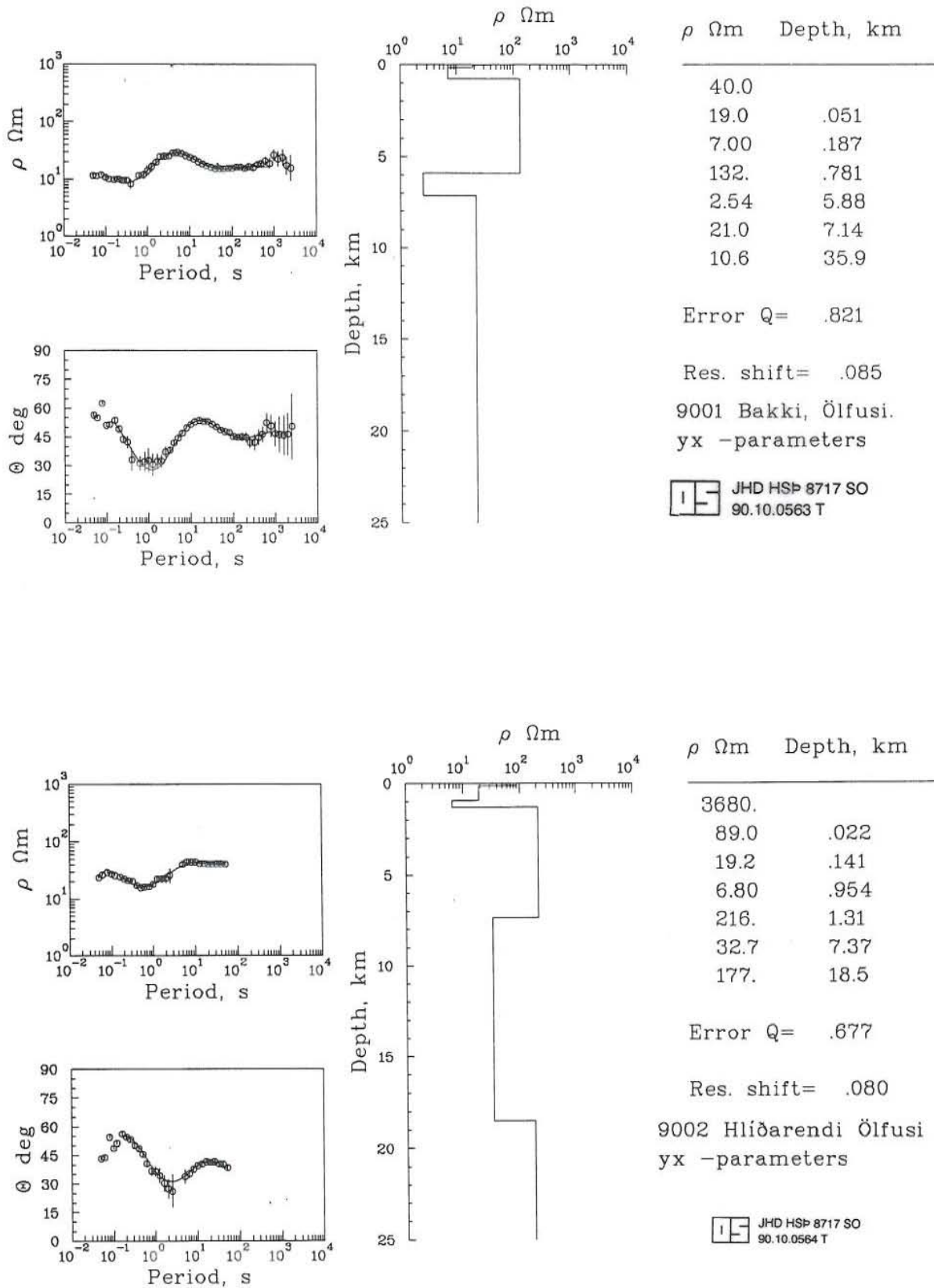FIGURE 23: 1-D TEM and MT resistivity section along profile AA' from Hlidarendi to Bakki

FIGURE 22: Seven layer inversion models for E polarization for MT sites 9001 and 9002
(direction of fixed rotation is 30°)

3.4   Discussions

The combined interpretation of DC Schlumberger, TEM and MT data has yielded some interesting results of the resistivity structure and its relationship with geophysical parameters and geological structure.

The low resistivity layer in the uppermost kilometre is found mainly in hyaloclastites and the temperatures are between 100° and 150°C (Figure 23). Most of the productive feeder zones are found within this permeable layer. The resistivity structure is generally affected by the percolation of saline seawater. Since there is no increase in resistivity below 600 m at site AÖ18 (Figure 18) unlike at all the other sites, one may expect that below this site there is a zone of vertical permeability that may be related to the upflow of geothermal fluids. However, it should be noted that the data from this site is rather noisy due to fences and power lines and, therefore, more data is needed to evaluate this proposition.

There is a correlation between the resistivity and the degree of hydrothermal alteration. The low resistivity in the hyaloclastite layer is associated with laumontite-wairakite zone while the higher resistivity below the low resistivity occurs in the epidote zone in association with basalts (Fridleifsson, 1990).

A deep low resistivity layer has been found in the neovolcanic zone in S-Iceland. It has been attributed to the presence of a basaltic partial melt at temperatures of 1100 to 1300°C and a melt fraction of 10-20% (Hersir et al., 1984; Eysteinsson and Hermance, 1985). Similar deep low resistivity in the Roosevelt hot springs thermal area have also been attributed to a partially molten magma chamber that might be the heat source for the geothermal system (Ward and Wannamaker, 1983). The deep low resistivity layer at Bakki may be either a part of the regional feature of the neovolcanic zone or a localized structure. The relationship between this deep low resistivity and the geothermal manifestations at Bakki is not clear. More data is needed to confirm the existence and extent of this layer at Bakki.

4. CONCLUSIONS AND RECOMMENDATIONS

The electrical methods are effective in evaluating the resistivity structure that may be related to the physio-chemical characteristics of the geothermal fields. The modelled resistivity structures relate directly to temperature, permeability, degree of hydrothermal alteration and geological and tectonic structures. The resolution of the model parameters depends on the electric method used and the procedures of interpretation. The 2-D modelling of the Schlumberger soundings from Eburru has given a better resolution of the lateral and vertical resistivity boundaries. The model has shown that the Eburru geothermal field is confined to the crater region and is mainly controlled by vertical permeability. The near-surface low resistivity is related to the effects of outflows along near-surface fractures and hydrothermal alteration of pyroclastics by acidic steam condensates. However, the 2-D model has not resolved the deeper structure below the conductive layer in the Eburru crater area and the Badlands.

The TEM method has given good resolution of the resistivity structure in the uppermost kilometre at Bakki. The low resistivity layer at a depth of 200 to 850 m is the main feeder zone for geothermal water at a temperature of 100° to 150°C. The low resistivity below 600m at site AÖ18 may related to the upflow zone of the Bakki geothermal field. This method is less sensitive to small scale inhomogeneities and has been used effectively to constrain the inversion of MT data. The TEM method has also been used to gain insight into the nature of MT shifts. The shifts vary from site to site but they are more than a decade (down) at the two sites in the Bakki area. The results of the combined interpretation of the TEM and MT methods show a deep (>5 km) low resistivity layer at Bakki that may be related to the heat source.

It is recommended that either a combined approach of DC Schlumberger, TEM and MT methods or a detailed 2-D Schlumberger interpretation augmented by MT be utilized in future projects in defining the lateral and horizontal boundaries of geothermal fields in Kenya. A detailed 2-D interpretation of the Badlands anomaly should be carried out. In the Bakki area of S-Iceland, a detailed combined interpretation of TEM and MT soundings should be carried out to investigate the main upflow zone and the extent of the deep low resistivity. The interpretation of the MT data should also involve a quantitative investigation of the ocean effects and the shifts on the data.

ACKNOWLEDGEMENTS

REFERENCES

Arnason, K., 1984: The effect of finite electrode separation on Schlumberger soundings. 54th Annual International SEG meeting Atlanta, Extended Abstracts, 129-132.

Arnason, K., 1989: Central loop transient electromagnetic soundings over a horizontally layered earth. Orkustofnun, report OS-89032/JHD-06, Reykjavik, 128 pp.

Bannister, P. R., 1969: Source distance dependence of the surface impendence conductivity measurement technique. Geophys., 34, 785-788.

Clarke, J., Gamble, T. D., Goubau, W. M., Koch, R. H. and Miracky, R. F., 1983: Remote reference magnetotellurics: Equipment and procedures. Geophys. prosp., 31, 149-170.

Drury, M. J. and Hyndman, R. D., 1979: The electric resistivity of ocean basalts. Jour. Geophys. Res., 84, 4537-4545.

Eysteinsson, H. and Hermance, J. F., 1985: Magnetotelluric measurements across the eastern neovolcanic zone in S-Iceland. Jour. Geophy. Res., 90, 10,093-10, 108.

Eysteinsson, H., 1988: The inversion of 2-D magnetotelluric and magnetic variation data. Ph.D. thesis, Brown University, Rhode Island, 385 pp.

Fontes, S. L., Harinarayana, T., Dawes, G. J. K. and Hutton, V. R. S., 1988: Processing of noisy MT data using digital filters and additional data selection criteria. Phys. Earth Planet Inter., 52, 30-40.

Flovenz, O. G., Georgsson, L. S. and Arnason, K., 1985: Resistivity structure of the upper crust in Iceland. Jour. of Geophy. Res., 90, 10.136-10.150.

Fridleifsson, G. O., 1990: Hydrothermal systems and associated alteration in Iceland. Proc. of the third Sym. on deep crust fluids, Mining Geol., Japan, in prep.

Georgsson, L. S., 1989: Bakki and Litlaland in Olfus, S-Iceland, TEM soundings in the summer 1989. Orkustofnun, report OS-89054/JHD-263 (in Icelandic), Reykjavik, 10 pp.

Group Seven Inc., 1972: Electric resistivity survey in the Rift Valley, Kenya. UNDP report.

Hattingh, M., 1989: The use of data adaptive filtering for noise removal on magnetotelluric data. Phys. of the Earth Planet Inter., 53, 239-254.

Hersir, G. P., Bjornsson, A. and Pedersen, L. B., 1984: Magnetotelluric survey across the active spreading zone in SW-Iceland. Jour. Volcanol. Geotherm. Res., 20, 253-265.

Hoversten, G. M. and Morrison, H. F., 1982: Transient fields of a current loop source above a layered earth, Geophy., 47, 1068-1077.

Ingham, M. R., 1988: The use of invariant impedances in magnetotelluric interpretation. Geophy. Jour., 92, 165-169.

JICA, 1983: Prefeasibility study report for the Rift Valley Geothermal development project in Kenya. JICA, report, 55 pp.

Jones, A. G. and Hutton, V.R.S., 1979: A multi station magnetotelluric study in southern Scotland, II Monte-Carlo inversion of the data and its geophysical and tectonic implications. Geophy. Jour. Roy. Astr. Soc., 56, 351-368.

Jones, A. G., 1988: Static shift of magnetotelluric data and its removal in a sedimentary basin environment. Geophy., 53, 967-978.

Kaufman, A. A. and Keller, G. V., 1983: Frequency and transient soundings. Elsevier, Amsterdam, 685 pp.

KPC, 1986: Scientific review and well siting meeting. KPC report prepared by GENZEL, Auckland.

Kristmannsdottir, H., Olafsson, M., Sigvaldason, H. and Tulinius, H., 1990. Exploitation induced influx of cold local groundwater into the geothermal system at Bakki, S-Iceland. Geothermal Resources Council, transactions 14 , 715-720.

Ku, C. C., Hsieh, M. S. and Lim, S. H., 1973: The topographic effect in electromagnetic fields. Can. Jour. of Earth Sci., 10, 645-656.

McNeill, J. D., Edwards, R. N. and Levy, G. M., 1984: Approximate calculations of the transient electromagnetic response from buried conductors in a conductive half-space. Geophy.,49, 918-924.

Muchemi, G. G., 1990: The geology of Eburru. KPC internal report, Kenya, 25 pp.

Nabighian, M. N., 1979: Quasi-static transient response of a conducting half-space. An approximate representation. Geophy., 44, 1700-1705.

Newman, G. A., Anderson, W. L. and Hohmann, G. W., 1987: Interpretation of transient electromagnetic soundings over three dimensional structures for the central loop configuration. Geophys. Jour. R. Astr. Soc., 89, 889-914.

Onacha, S. A., 1990: The electric resistivity structure of the Eburru prospect. KPC internal report, Kenya, 18 pp.

Ranganayaki, R. P., 1984: An interpretive analysis of magnetotelluric data. Geophy. 49, 1730-1748.

Simiyu, S. M., 1990: The gravity structure of Eburru, Kenya. UNU G.T.P., Iceland, report 13, 39 pp.

Sternberg, B. K., Washburne, J. C. and Pellerin, L., 1988: Correction for the static shift in magnetotelluric using transient electromagnetic soundings. Geophy., 53, 1459-1468.
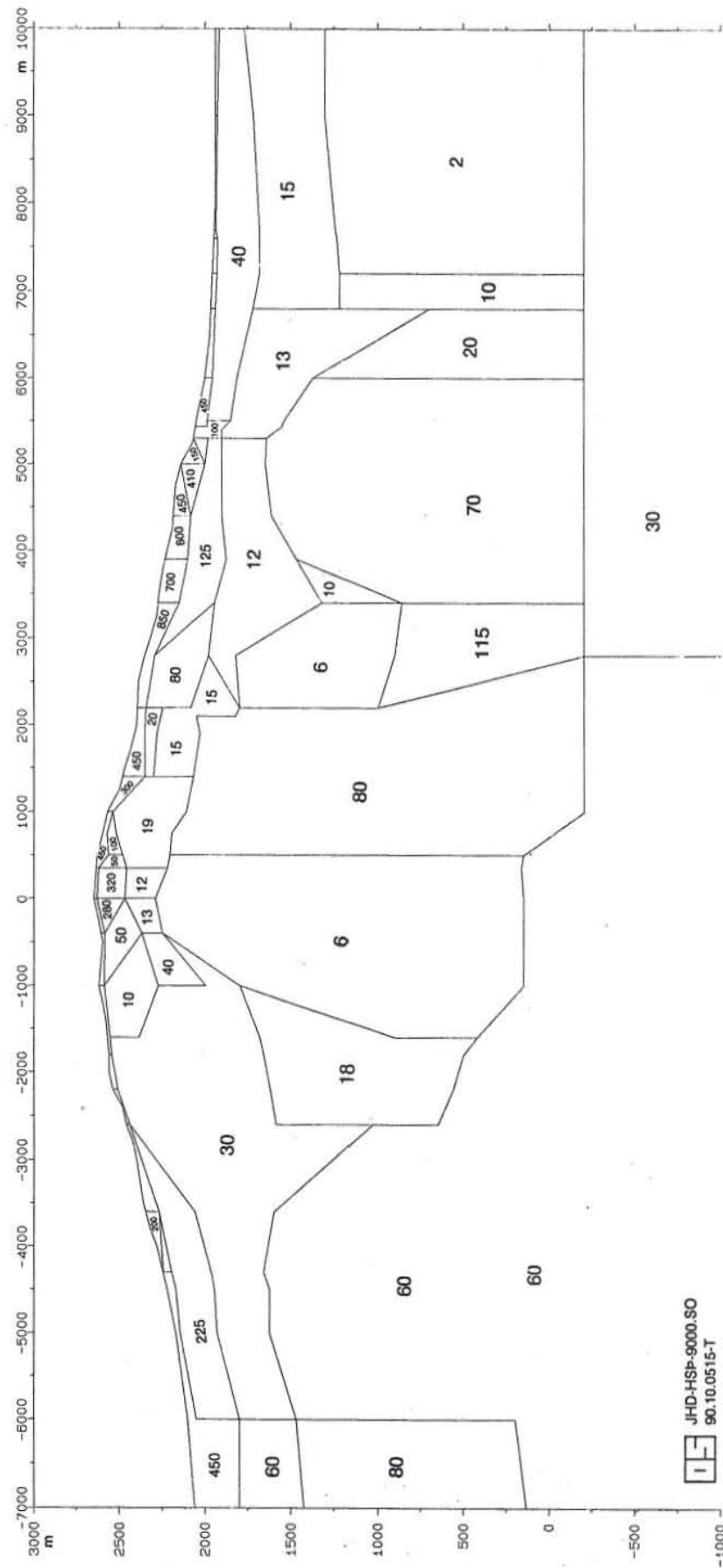
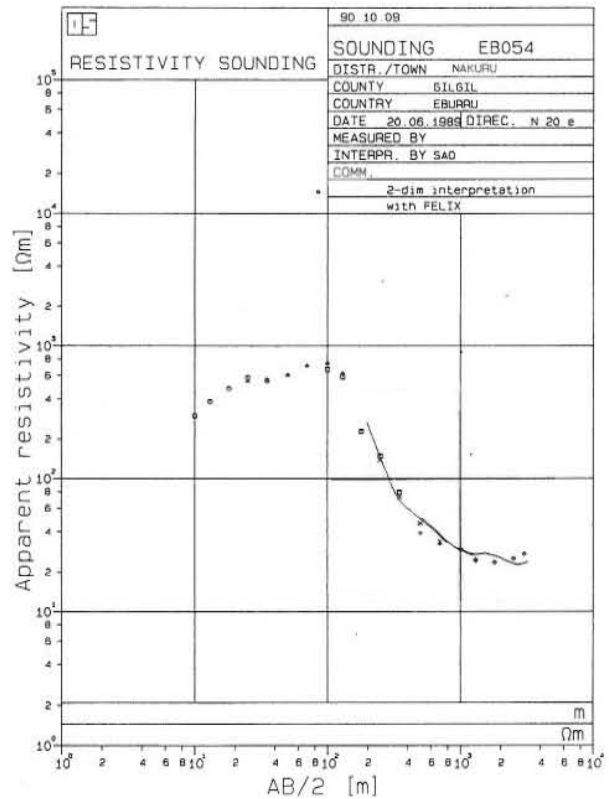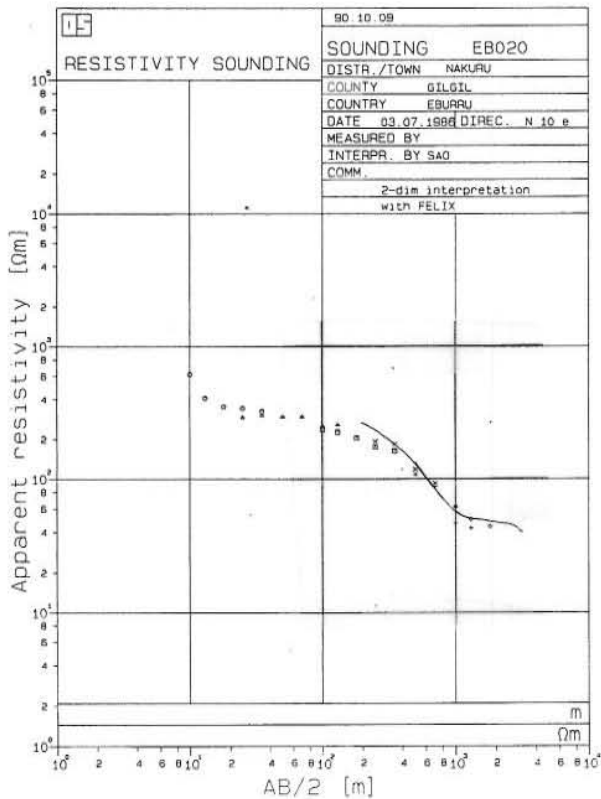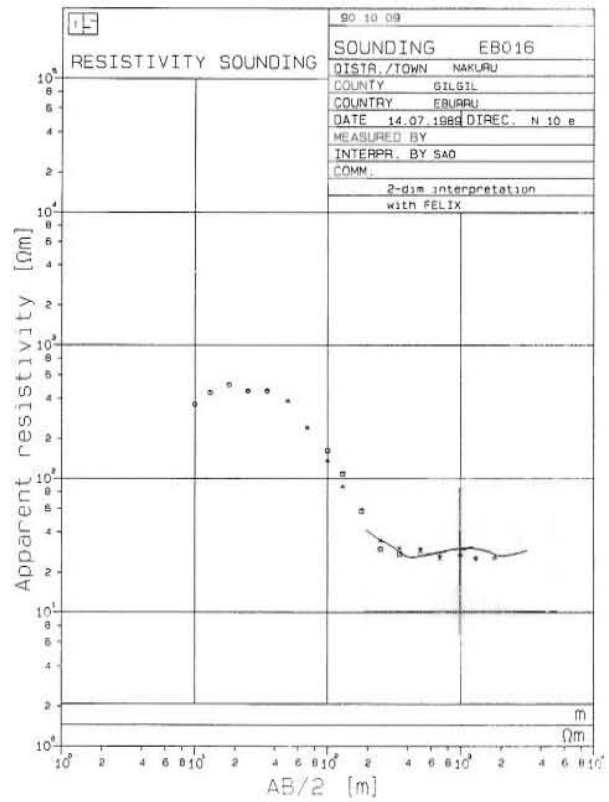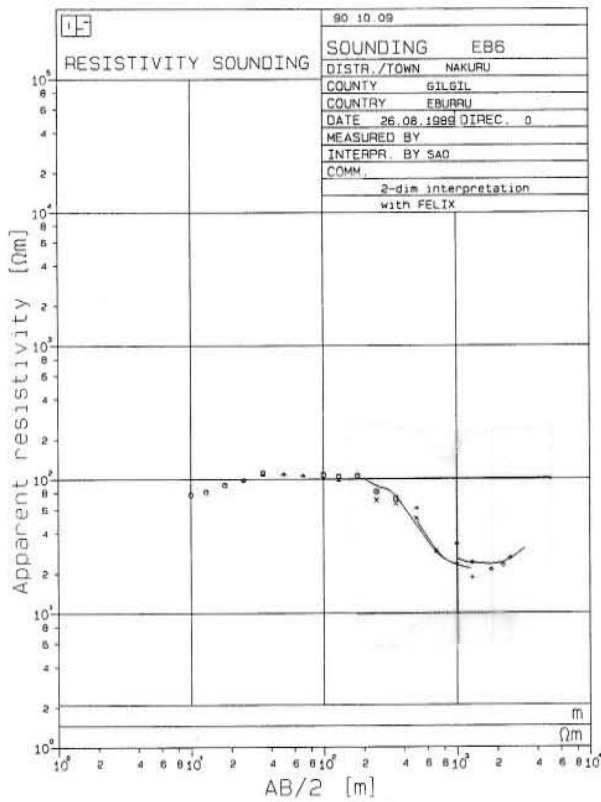Vozoff, K., 1972: The magnetotelluric method in the exploration of sedimentary basins. Geophy., 37, 98-141.

Ward, S. H. and Wannamaker, P. E., 1983: The MT/AMT electromagnetic method in geothermal exploration. UNU G.T.P., Iceland, report 5, 107 pp.

Ward, S. H. and Hohmann, G. W., 1988: Electromagnetic theory for geophysical applications. In: Electromagnetic methods in applied geophysics - Theory, SEG, Tulsa, Oklahoma, 513 pp.
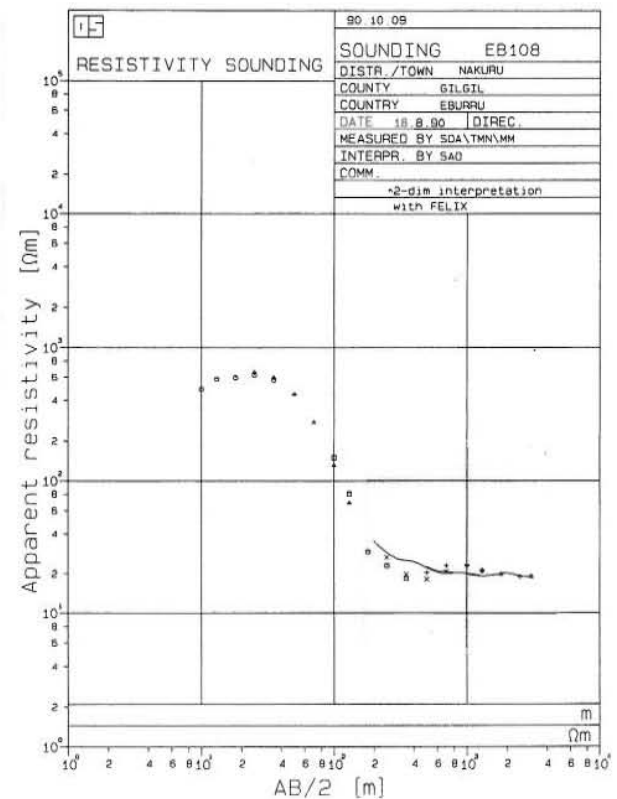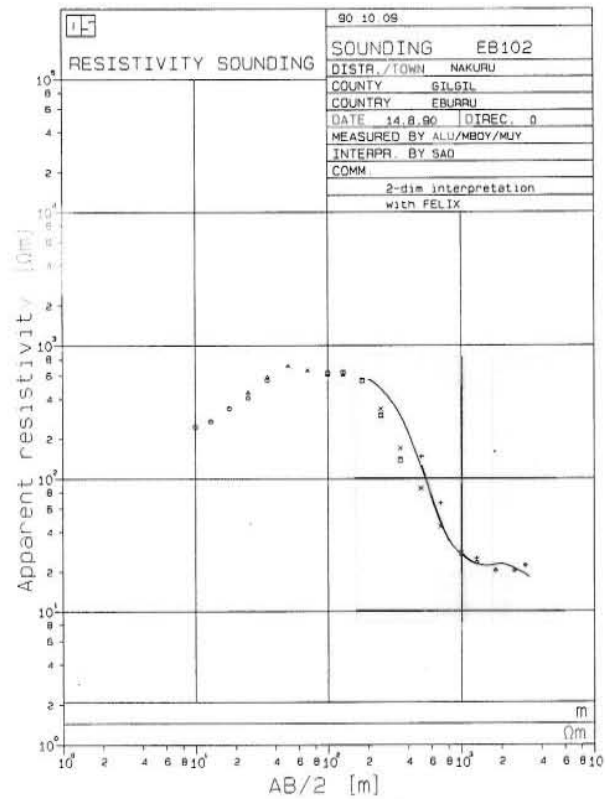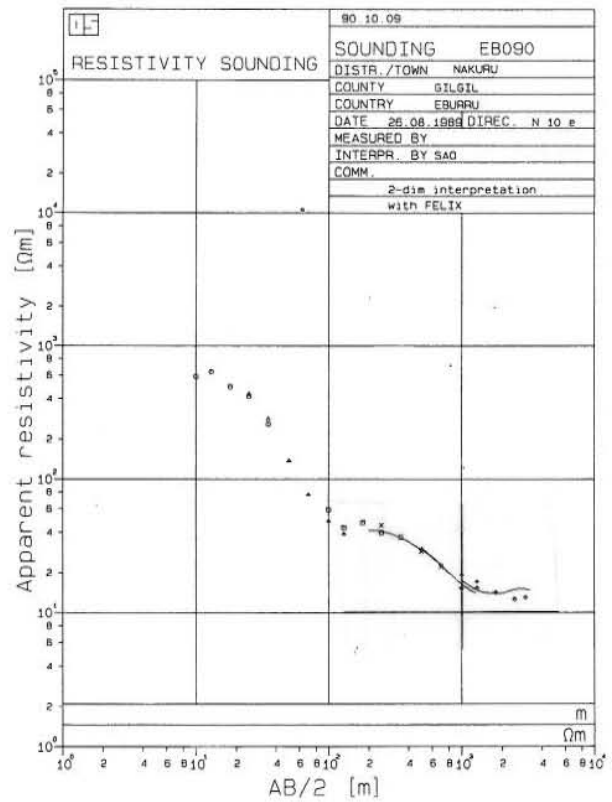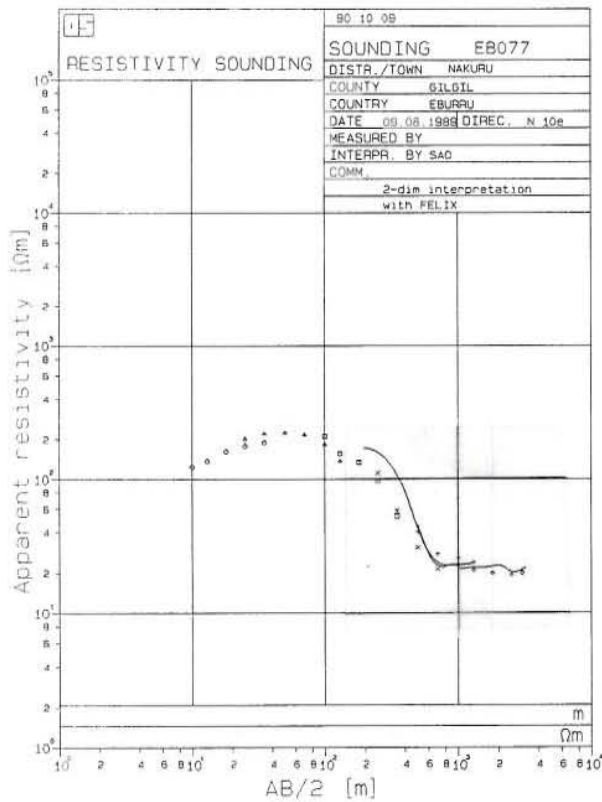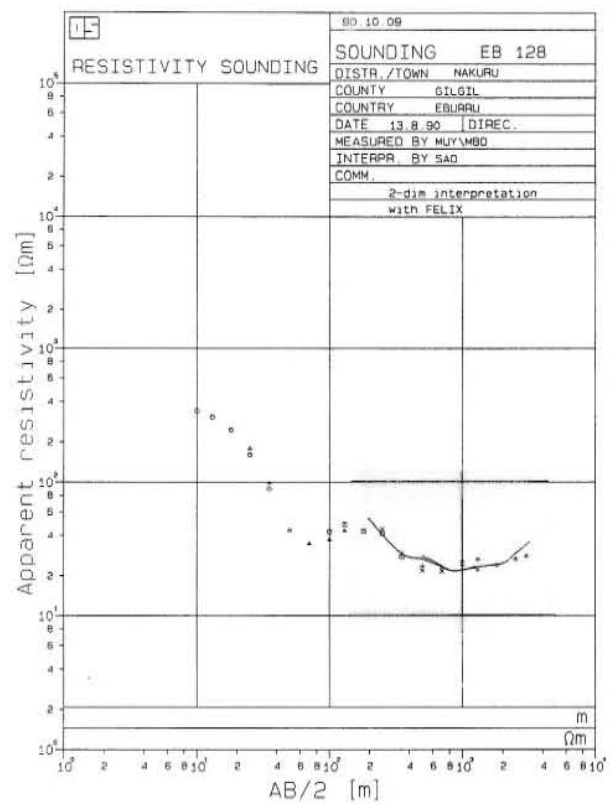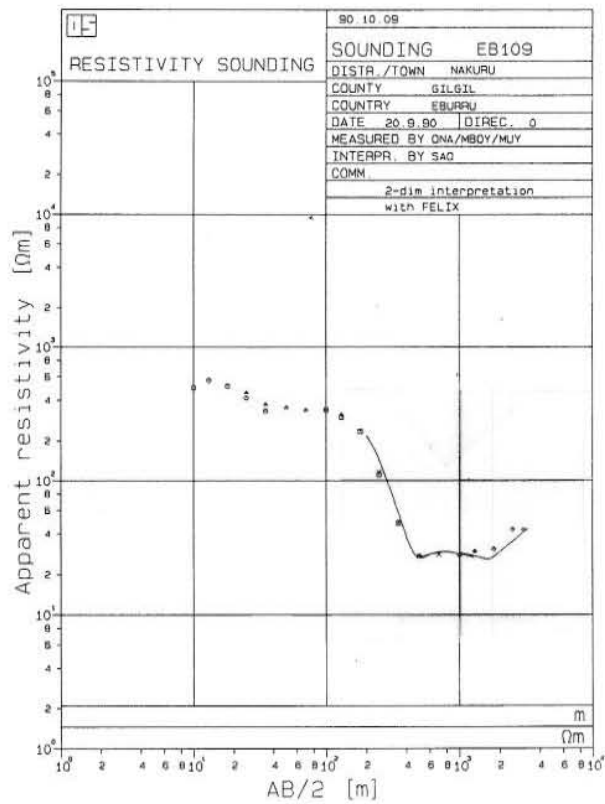
APPENDIX A: 2-D resistivity model of profile AB, and Schlumberger data with 2-D model curves

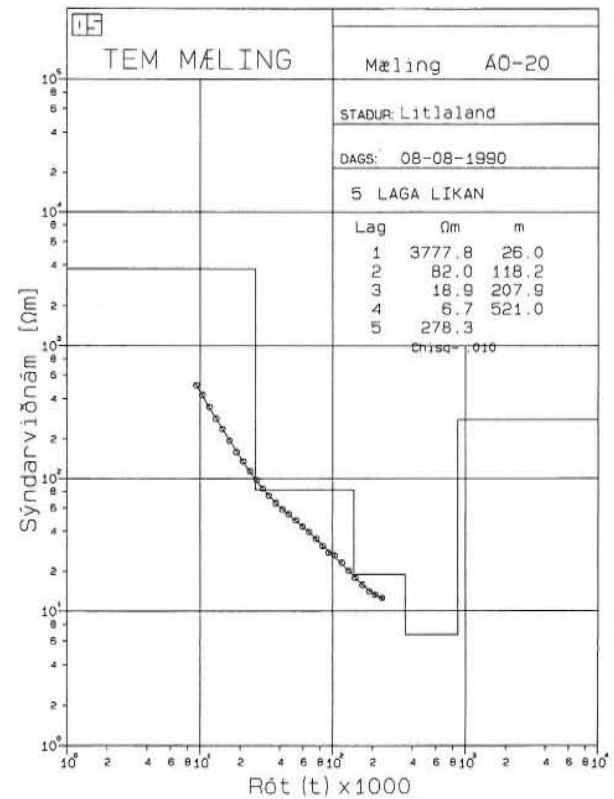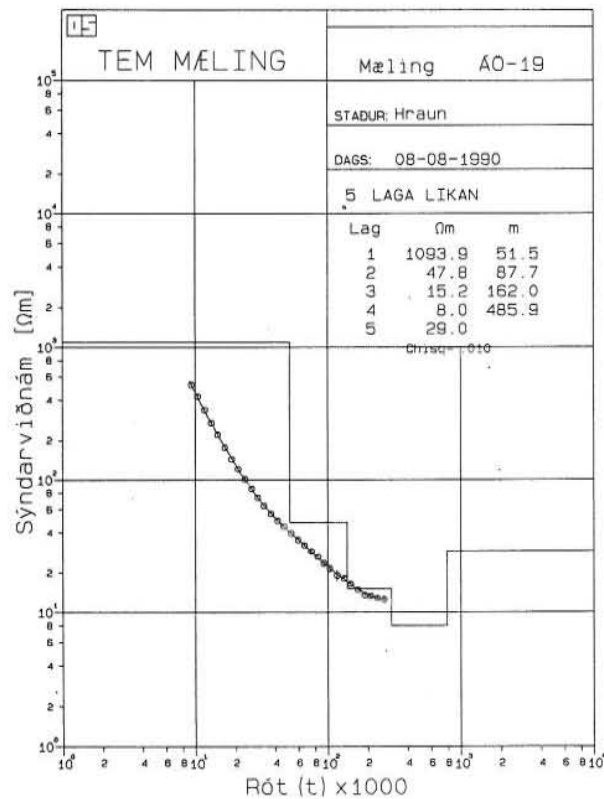46

RESISTIVITY SOUNDING

90 10 09

SOUNDING   EB077
DISTR./TOWN   NAKURU
COUNTY   GILGIL
COUNTRY   EBURRU
DATE   09.08.1989 DIREC.   N 10e
MEASURED BY
INTERPR. BY SAO
COMM.
2-dim interpretation
with FELIX

Apparent resistivity [Ωm]

AB/2 [m]

RESISTIVITY SOUNDING

90 10 09

SOUNDING   EB090
DISTR./TOWN   NAKURU
COUNTY   GILGIL
COUNTRY   EBURRU
DATE   26.08.1989 DIREC.   N 10 e
MEASURED BY
INTERPR. BY SAO
COMM.
2-dim interpretation
with FELIX

Apparent resistivity [Ωm]

AB/2 [m]

RESISTIVITY SOUNDING

90 10 09

SOUNDING   EB102
DISTR./TOWN   NAKURU
COUNTY   GILGIL
COUNTRY   EBURRU
DATE   14.8.90   DIREC.   0
MEASURED BY ALU/MBOY/MUY
INTERPR. BY SAO
COMM.
2-dim interpretation
with FELIX

Apparent resistivity [Ωm]

AB/2 [m]

RESISTIVITY SOUNDING

90 10 09

SOUNDING   EB108
DISTR./TOWN   NAKURU
COUNTY   GILGIL
COUNTRY   EBURRU
DATE   18.8.90   DIREC.
MEASURED BY SOA\TMN\MM
INTERPR. BY SAO
COMM.
-2-dim interpretation
with FELIX

Apparent resistivity [Ωm]

AB/2 [m]

RESISTIVITY SOUNDING

SOUNDING   EB109
DISTR./TOWN   NAKURU
COUNTY   GILGIL
COUNTRY   EBURRU
DATE   20.9.90   DIREC. 0
MEASURED BY ONA/MBOY/MUY
INTERPR. BY SAO
COMM.
2-dim interpretation
with FELIX

Apparent resistivity [Ωm]
AB/2 [m]

RESISTIVITY SOUNDING

SOUNDING   EB 128
DISTR./TOWN   NAKURU
COUNTY   GILGIL
COUNTRY   EBURRU
DATE   13.8.90   DIREC.
MEASURED BY MUY\MBO
INTERPR. BY SAO
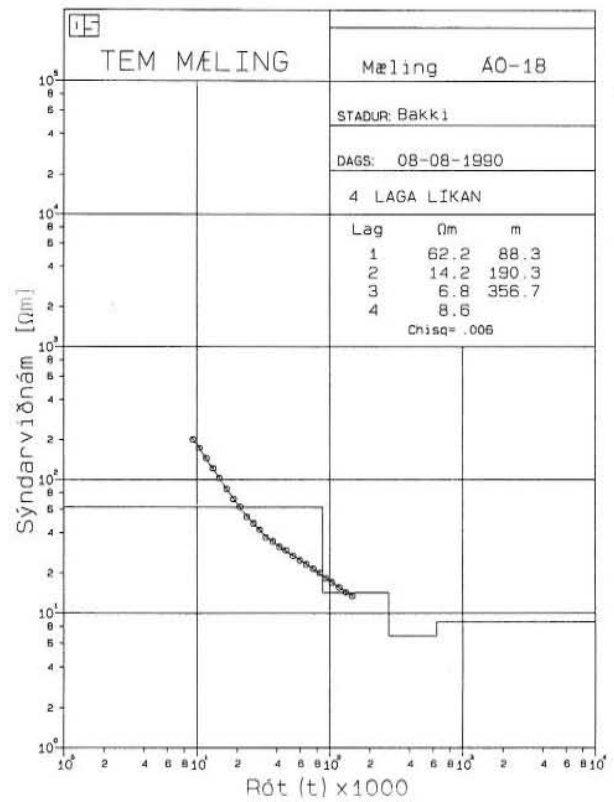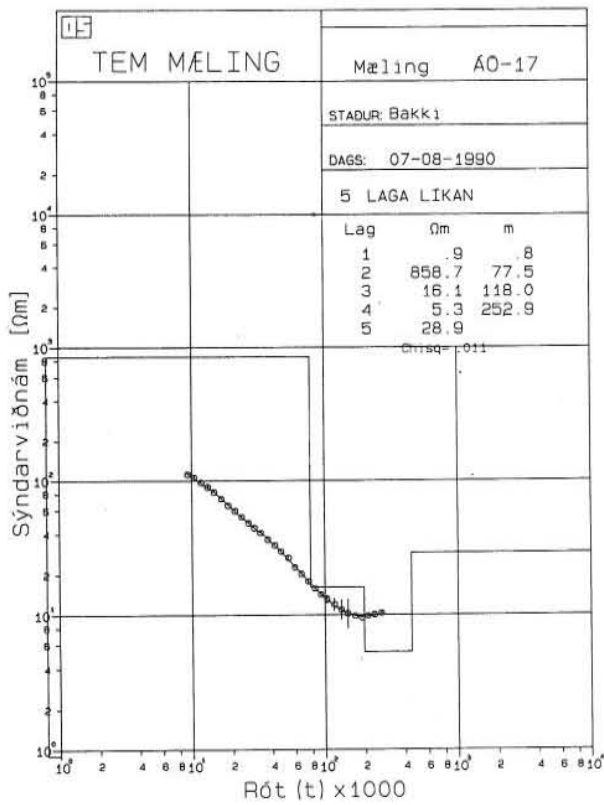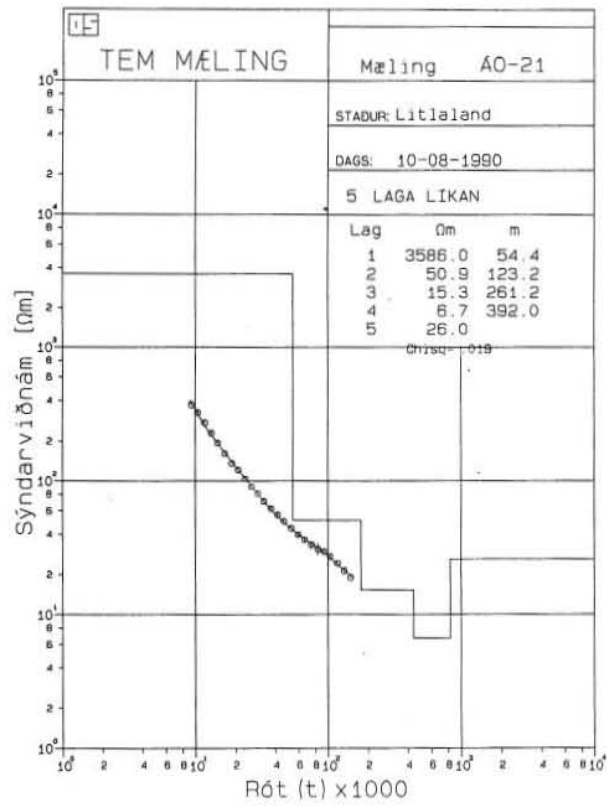COMM.
2-dim interpretation
with FELIX

Apparent resistivity [Ωm]
AB/2 [m]

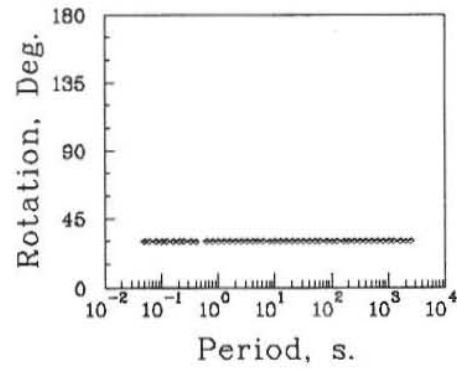# APPENDIX B: TEM data from Bakki in Olfus with 1-D model curves

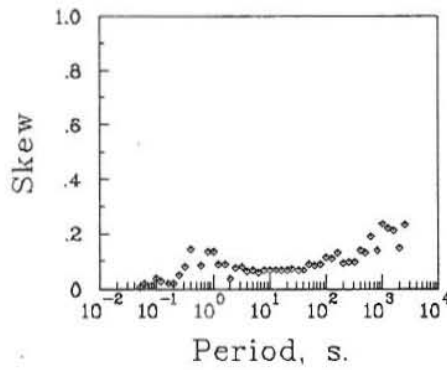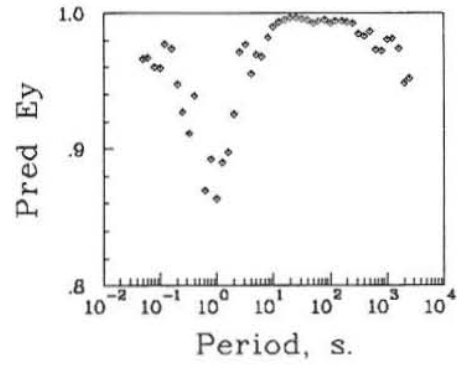TEM MÆLING — Mæling ÁO-17
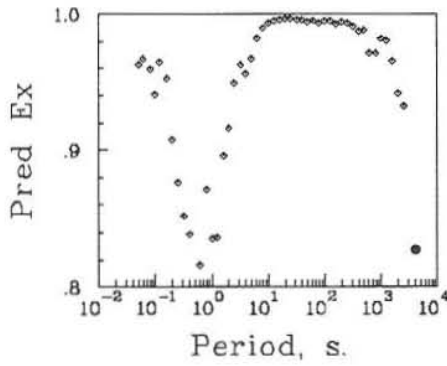
STADUR: Bakki

DAGS: 07-08-1990

5 LAGA LIKAN

Lag	Ωm	m
1	.9	.8
2	858.7	77.5
3	16.1	118.0
4	5.3	252.9
5	28.9	

Chisq= .011

TEM MÆLING — Mæling ÁO-18

STADUR: Bakki

DAGS: 08-08-1990

4 LAGA LIKAN

Lag	Ωm	m
1	62.2	88.3
2	14.2	190.3
3	6.8	356.7
4	8.6	

Chisq= .006

TEM MÆLING — Mæling ÁO-19

STADUR: Hraun

DAGS: 08-08-1990

5 LAGA LIKAN

Lag	Ωm	m
1	1093.9	51.5
2	47.8	87.7
3	15.2	162.0
4	8.0	485.9
5	29.0	

Chisq= .010

TEM MÆLING — Mæling ÁO-20

STADUR: Litlaland

DAGS: 08-08-1990

5 LAGA LIKAN

Lag	Ωm	m
1	3777.8	26.0
2	82.0	118.2
3	18.9	207.9
4	6.7	521.0
5	278.3	

Chisq= .010

TEM MÆLING

Mæling   ÁO-21

STADUR: Litlaland

DAGS: 10-08-1990

5 LAGA LÍKAN

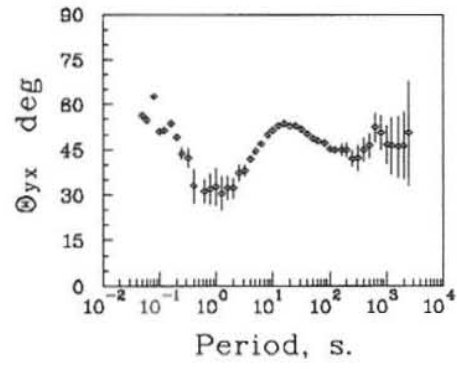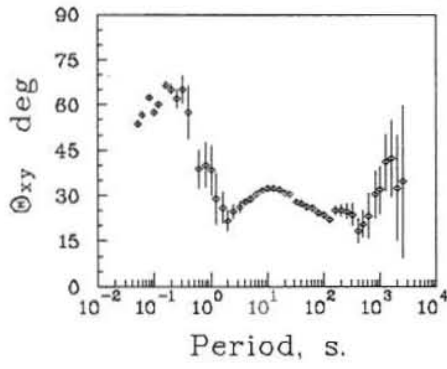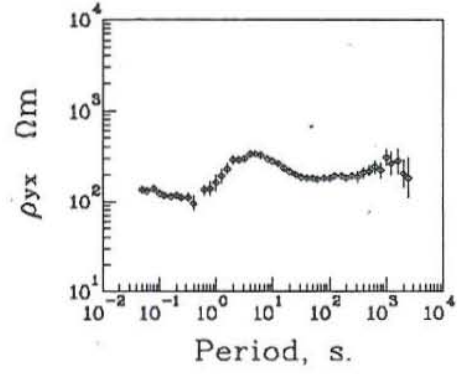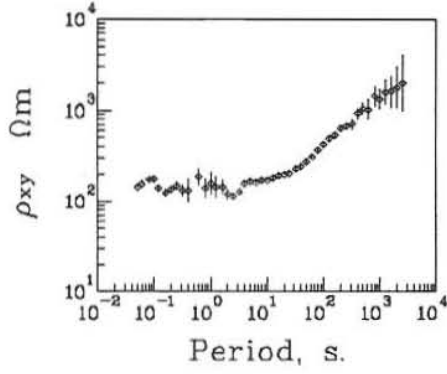| Lag	Ωm	m
1	3586.0	54.4
2	50.9	123.2
3	15.3	261.2
4	6.7	392.0
5	26.0	

Chisq= .018

Sýndarviðnám [Ωm]

Rót (t) ×1000

APPENDIX C: AMT/MT data from Bakki in Olfus

9001

9002